VAMP8-dependent fusion of recycling endosomes with the plasma membrane facilitates T lymphocyte cytotoxicity

Misty R. Marshall,[1,4] Varsha Pattu,[1] Mahantappa Halimani,[1,6] Monika Maier-Peuschel,[1] Martha-Lena Müller,[4] Ute Becherer,[1] Wanjin Hong,[5] Markus Hoth,[2] Thomas Tschernig,[3] Yenan T. Bryceson,[4]* and Jens Rettig[1]*

[1]Cellular Neurophysiology, Center for Integrative Physiology and Molecular Medicine, [2]Department of Biophysics, and [3]Department of Anatomy, Saarland University, 66421 Homburg, Germany
[4]Department of Medicine, Center For Infectious Medicine, 14186 Stockholm, Sweden
[5]Membrane Biology Laboratory, Institute of Molecular and Cell Biology, Singapore 138673
[6]Department of Pathology, Brigham and Woman's Hospital, Boston, MA

Cytotoxic T lymphocytes (CTLs) eliminate infected and neoplastic cells through directed release of cytotoxic granule contents. Although multiple SNARE proteins have been implicated in cytotoxic granule exocytosis, the role of vesicular SNARE proteins, i.e., vesicle-associated membrane proteins (VAMPs), remains enigmatic. VAMP8 was posited to represent the cytotoxic granule vesicular SNARE protein mediating exocytosis in mice. In primary human CTLs, however, VAMP8 colocalized with Rab11a-positive recycling endosomes. Upon stimulation, these endosomes rapidly trafficked to and fused with the plasma membrane, preceding fusion of cytotoxic granules. Knockdown of VAMP8 blocked both recycling endosome and cytotoxic granule fusion at immune synapses, without affecting activating signaling. Mechanistically, VAMP8-dependent recycling endosomes deposited syntaxin-11 at immune synapses, facilitating assembly of plasma membrane SNARE complexes for cytotoxic granule fusion. Hence, cytotoxic granule exocytosis is a sequential, multivesicle fusion process requiring VAMP8-mediated recycling endosome fusion before cytotoxic granule fusion. Our findings imply that secretory granule exocytosis pathways in other cell types may also be more complex than previously appreciated.

Introduction

Cytotoxic T lymphocytes (CTLs) together with natural killer cells can recognize and kill infected and neoplastic cells. Killing by these cell types is mediated by exocytosis of specialized secretory lysosomes, called cytotoxic granules, which contain the cytotoxic proteins perforin and granzymes (Trapani and Smyth, 2002; Stinchcombe and Griffiths, 2007; de Saint Basile et al., 2010). CTL activation is dictated by somatically recombined, clonally distributed T cell receptors (TCRs) that bind specific complexes of peptide major histocompatibility complex (pMHC) molecules on target cells. Upon engagement, CTLs can induce target cell death within minutes (Lopez et al., 2013). The immune synapse is a spatially organized site of contact between CTLs and target cells, supporting both directed exocytosis of cytotoxic granules and signaling required for cytokine production (Dustin and Long, 2010). For CTLs, induction of an immune synapse and full activation requires at least 10 pMHC complexes on the target cell (Purbhoo et al., 2004). However, three pMHCs are sufficient to facilitate transient interactions that support target cell killing without formation of a mature immune synapse (Sykulev et al., 1996; Faroudi et al., 2003; Purbhoo et al., 2004). Thus, CTL killing is rapid, extremely sensitive to antigen, and involves a complex intracellular signaling cascade that polarizes proteins required for cytotoxic granule exocytosis toward the target cell interface.

In eukaryotes, exocytosis as well as intracellular vesicle fusion processes is mediated by transmembrane proteins containing cytoplasmic SNARE domains (Jahn and Scheller, 2006; Südhof and Rothman, 2009). Typically, one R-SNARE protein residing on the vesicular membrane and three Q-SNAREs (Qa, Qb, and Qc) proteins residing on the target membrane can span the distance between two membranes, forming a parallel

*Y.T. Bryceson and J. Rettig contributed equally to this paper.

Correspondence to Jens Rettig: jrettig@uks.eu; or Yenan T. Bryceson: Yenan.Bryceson@ki.se

Abbreviations used in this paper: ANOVA, analysis of variance; CMV, cytomegalovirus; CTL, cytotoxic T lymphocyte; ERK, extracellular signal–regulated kinase; HLH, hemophagocytic lymphohistiocytosis; MFI, mean fluorescence intensity; PBMC, peripheral blood mononuclear cell; pMHC, peptide major histocompatibility complex; qRT-PCR, quantitative real-time PCR; SEA, superantigen staphylococcal enterotoxin A; SIM, structured illumination microscopy; Stx11, syntaxin-11; TCR, T cell receptor; TIRF, total internal reflection fluorescence; VAMP, vesicle-associated membrane protein.

The Rockefeller University Press $30.00
J. Cell Biol. Vol. 210 No. 1 135–151
www.jcb.org/cgi/doi/10.1083/jcb.201411093

four-helical bundle that catalyzes membrane fusion (Sutton et al., 1998). When forming a SNARE complex, SNARE proteins evince remarkable specificity for their cognate SNARE partners, resulting in highly specific combinations of SNAREs at differing steps of vesicle fusion (Chen and Scheller, 2001; Ungermann and Langosch, 2005).

Whereas SNARE-dependent exocytosis has been extensively studied in the context of neurotransmitter release, current research shows that SNARE-dependent exocytosis is also critical for proper immunological function (Stow et al., 2006). Mutations in genes encoding the SNARE protein syntaxin-11 (Stx11) and SNARE complex regulators Munc13-4 and Munc18-2, as well as the gene encoding perforin, are all associated with development of an early onset, often fatal, hyperinflammatory syndrome termed hemophagocytic lymphohistiocytosis (HLH; Stepp et al., 1999; Feldmann et al., 2003; zur Stadt et al., 2005, 2009; Côte et al., 2009). Importantly, Stx11, Munc13-4, or Munc18-2 deficiency abrogates cytotoxic granule exocytosis and target cell killing by CTL (Bryceson et al., 2007; Côte et al., 2009; zur Stadt et al., 2009). In Stx11-deficient cytotoxic lymphocytes, cytotoxic granules polarize to the target cell interface but fail to fuse with the plasma membrane (Bryceson et al., 2007), suggesting that Stx11 mediates cytotoxic granule fusion for target cell killing. With the exception of Stx11, other members of the SNARE complex regulating cytotoxic granule fusion with the plasma membrane have not been clearly defined, although several SNARE-containing candidates have been proposed (Stow, 2013). Conjointly, Munc13-4 has also been shown to facilitate intermediate steps of cytotoxic granule maturation, promoting late endosome-to-lysosome fusion (Ménager et al., 2007), suggesting that multiple vesicle fusion steps regulate cytotoxic granule exocytosis and hence, several SNARE complexes might control cytotoxic granule exocytosis.

The vesicle-associated membrane protein (VAMP) family typically mediates fusion of vesicles with cognate, membrane-associated SNARE complexes, and several VAMPs have been implicated in lymphocyte cytotoxicity. *Vamp2* (encoding VAMP2 or synaptobrevin-2) knockout mice display defective cytotoxic granule exocytosis (Matti et al., 2013). Moreover, VAMP2 colocalizes with cytotoxic granules, indicating that VAMP2 may serve as a vesicular R-SNARE for cytotoxic granule exocytosis. Concurrently, VAMP4, and VAMP7 also colocalize with cytotoxic granule proteins and siRNA-mediated knockdown in a human natural killer cell line exhibited deficits in lymphocyte cytotoxicity (Krzewski et al., 2011). Furthermore, in mice, VAMP8, an R-SNARE associated with exocytosis of secretory pathway organelles in multiple immune cell types, colocalized with the cytotoxic granule protein granzyme B. *Vamp8* knockout mouse CTLs display reduced granule exocytosis and impaired target cell killing, also indicating that VAMP8 may be required for cytotoxic granule exocytosis (Loo et al., 2009; Dressel et al., 2010). Thus, how distinct VAMPs regulate cytotoxic granule trafficking and fusion for target cell killing is unclear.

Here, we studied the role of VAMP8 in cytotoxic granule fusion in primary human lymphocytes using structured illumination microscopy (SIM) and total internal reflection fluorescence (TIRF) microscopy. Examining endogenous as well as fluorescently tagged, ectopically expressed protein, we established that VAMP8 is associated with the recycling endosome compartment rather than with cytotoxic granules. Complimentary approaches revealed that recycling endosomes rapidly accumulated and fused at the immune synapse, preceding the arrival of cytotoxic granules. Strikingly, reduction of VAMP8 expression compromised both recycling endosome and cytotoxic granule fusion, delineating a VAMP8-dependent fusion step between recycling endosomes and the plasma membrane that brings Stx11 to the immune synapse for cytotoxic granule exocytosis. These insights provide a new mechanistic view of cytotoxic lymphocyte exocytosis and bear relevance to how VAMP8 may support regulated secretion in several other cell types.

Results

VAMP8 accumulates at the immune synapse of human CTL

We examined human CTL expression of VAMP8, which from studies of knockout mice has been suggested to represent the vesicular SNARE required for cytotoxic granule exocytosis. *VAMP8* transcripts were expressed in human primary $CD8^+$ T cells, and their levels increased upon anti-CD3 and anti-CD28 bead stimulation, as assessed by quantitative real-time PCR (qRT-PCR; Fig. 1 A). Upon anti-CD3 and anti-CD28 bead or superantigen staphylococcal enterotoxin A (SEA) stimulation, VAMP8 protein expression also increased (Fig. 1, B and C). Notably, in our model, increased expression of VAMP8 upon activation coincided with an increased capacity of the stimulated CTL to kill target cells (Pattu et al., 2012). As the proportion of unstimulated, bulk $CD8^+$ T cells expressing perforin and other cytotoxic granule constituents varies from donor to donor depending on the distribution of different cellular subsets (Chiang et al., 2013), we used $CD8^+$ T cells stimulated with beads or SEA that more homogeneously express cytotoxic granule constituents for all further experiments. Such cells are hereafter referred to as CTLs.

Studies in mice have indicated that VAMP8 is recruited to the immune synapse of CTLs (Loo et al., 2009). We found that numerous VAMP8-carrying vesicles also accumulated at the immune synapse of human CTL conjugated with SEA-pulsed target cells, as revealed by immunofluorescence microscopy and SIM (Fig. 1 D). SIM increases the spatial resolution of fluorescence microscopes to resolve colocalization within a resolution of 100 nm in x, y, and z direction (Gustafsson, 2005; Gustafsson et al., 2008). A similar accumulation of VAMP8 at immune synapses was observed upon expression of full-length VAMP8 fused to TFP (VAMP8-TFP) in target cell–conjugated CTL (Fig. 1 E). A twofold accumulation of endogenous and ectopically expressed TFP-tagged VAMP8, respectively (2.2 ± 0.2–fold and 2.0 ± 0.1–fold for endogenous VAMP8 vs. ectopically expressed VAMP8-TFP, $n = 10$ and 11 CTLs, respectively), toward target cells was observed. Notably, both VAMP8-TFP and VAMP8-mCherry constructs colocalized well with endogenous VAMP8, implying that these C-terminally tagged constructs properly localized to VAMP8-carrying vesicles (Fig. S1, A and B). These results suggest that VAMP8 may also play a role in cytotoxic granule exocytosis in human CTLs.

VAMP8 colocalizes with recycling endosomes rather than perforin-containing cytotoxic granules

We set out to decipher how VAMP8 may facilitate cytotoxic granule exocytosis. In contrast to studies of mouse CTL (Loo et al., 2009), we found VAMP8 localization to be distinct from

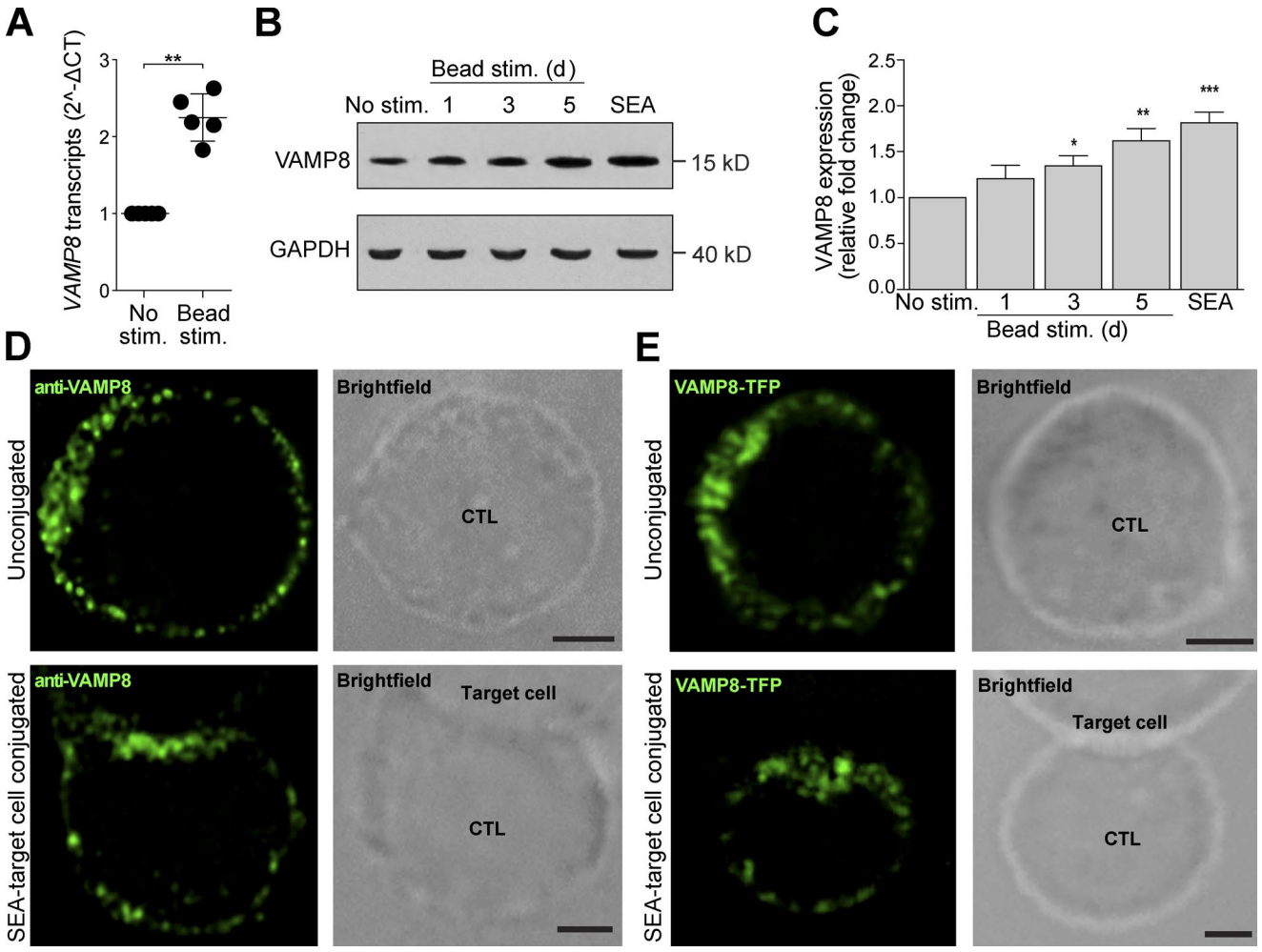

Figure 1. **Activation induces up-regulation of VAMP8 expression and polarization of VAMP8 to immune synapses in human CD8⁺ T cells.** (A) Relative expression of *VAMP8* transcripts in unstimulated or bead-stimulated (stim.) CD8⁺ T cells was determined by qRT-PCR. *UBC* (encoding ubiquitin C) transcripts were used for normalization. Graph depicts data from five individual donors (paired *t* test, **, P = 0.0035). (B) VAMP8 expression in naive, bead-stimulated for the indicated days, or SEA-stimulated for 5 d CD8⁺ T cells was determined by Western blot analysis. (C) Expression of VAMP8 relative to GAPDH in CD8⁺ T cells after various stimulations, as indicated. Graphs represent mean, normalized expression of VAMP8 in five individuals with SD indicated (paired *t* test, *, P < 0.05; **, P < 0.005; ***, P < 0.001). (D) SIM images of endogenous VAMP8 localization in unconjugated (top) and SEA-target cell-conjugated (bottom) CTLs. (E) SIM images of ectopically expressed VAMP8-TFP localization in unconjugated (top) and SEA-target cell-conjugated (bottom) CTLs. Bars, 2.5 µm.

that of granzyme B in unconjugated, fixed human primary CTLs using SIM (Fig. 2 A). Of note, VAMP8-carrying compartments were more numerous than those with granzyme B. Upon conjugation with SEA-pulsed target cells, VAMP8-carrying vesicles did not start to colocalize with those containing granzyme B (Fig. 2 B). Similarly, VAMP8-carrying vesicles did not colocalize with perforin-containing vesicles in unconjugated or conjugated CTLs (Fig. 2, C and D). Unexpectedly, we conclude that VAMP8 localized to a compartment distinct from cytotoxic granules in human CTLs.

Having established that VAMP8 did not colocalize with cytotoxic granules, we sought the identity of the endosomal compartment that did contain VAMP8. CTLs were transfected with VAMP8-TFP and various endosomal markers coupled to mCherry. CTLs were thereafter mixed with SEA-pulsed target cells, fixed, and imaged using SIM. Imaging revealed limited colocalization between VAMP8 and Rab5a, a marker of early endosomes (Rybin et al., 1996; Barysch et al., 2009), or Rab7a, a marker of late endosomes (Pearson's coefficient r of 0.34/0.39 and 0.36/0.36, respectively; Figs. 3 and S2; Chavrier et al., 1990). However, a substantial degree of colocalization was observed between VAMP8 and Rab11a, a marker of recycling endosomes (Ullrich et al., 1996), as indicated by a Pearson's coefficient of 0.68/0.72 in unconjugated and conjugated CTLs, respectively (Figs. 3 and S2). Overall, VAMP8 preferentially localized to recycling endosomes in CTLs, with its distribution not being drastically affected by stimulation. These findings raise questions of how VAMP8 may facilitate human lymphocyte cytotoxicity.

VAMP8-carrying recycling endosomes traffic and fuse with the plasma membrane at immune synapses

Although VAMP8 exhibited strong colocalization with recycling endosomes in our fixed cell experiments, it was unclear whether these VAMP8 vesicles were also trafficking through the recycling endosome compartment and fusing at the immune synapse. To examine the behavior of VAMP8-carrying vesi-

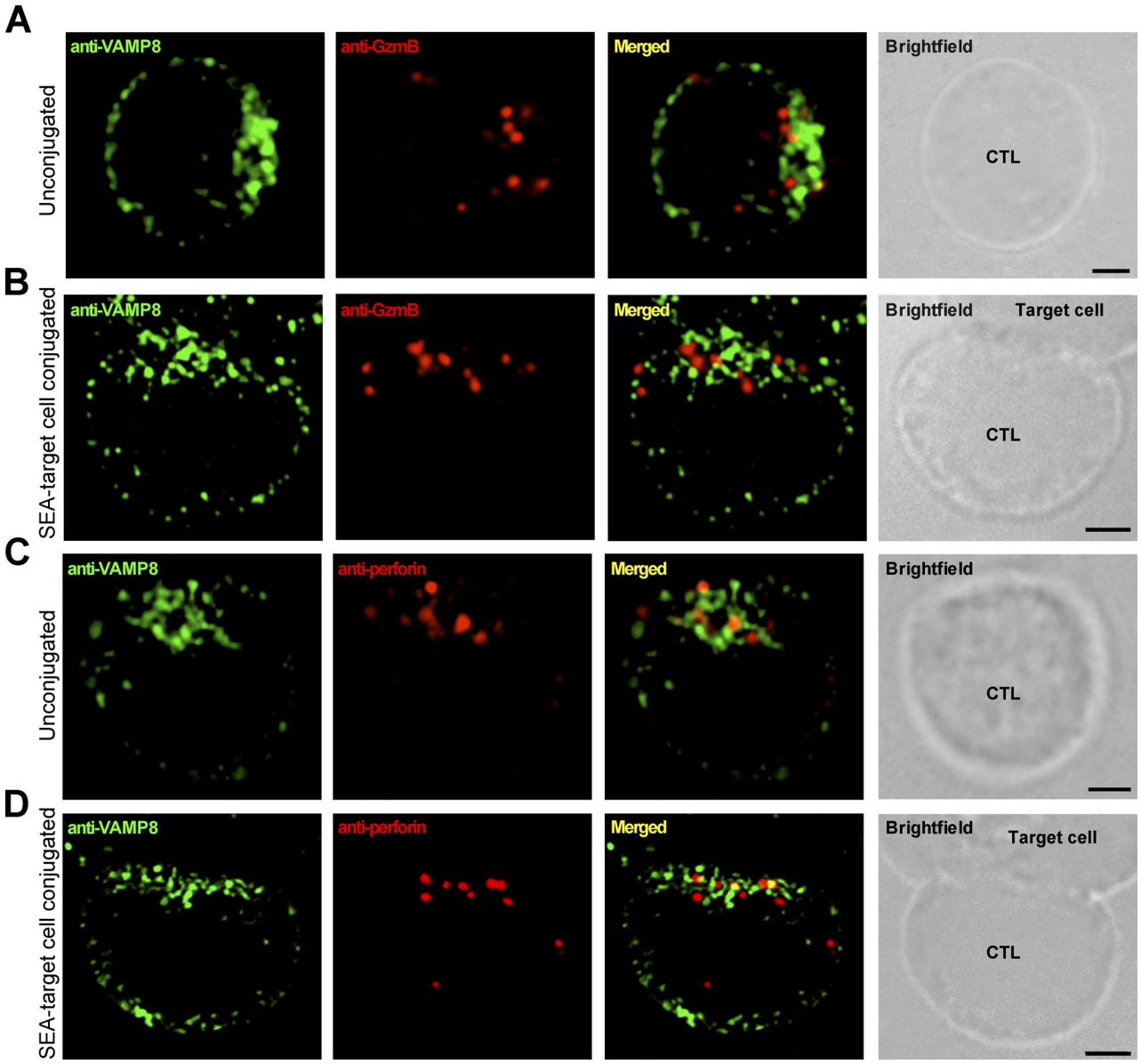

Figure 2. **VAMP8 does not colocalize with cytotoxic granule constituents in human CTLs.** (A and B) SIM images depicting VAMP8 localization in unconjugated (A) or SEA-target cell-conjugated (B) human CTLs stained with anti-VAMP8 and anti–granzyme B (GzmB). (C and D) SIM images depicting VAMP8 localization in unconjugated (C) or SEA-target cell-conjugated (D) CTLs stained with anti-VAMP8 and anti-perforin. (C) SIM images of resting human CTL stained with anti-VAMP8 and anti-perforin. For SEA-target cell-conjugated CTLs, the Pearson's coefficient for VAMP8 versus perforin was r = 0.28 (n = 10). Bars, 2.5 µm.

cles, we used TIRF microscopy to visualize vesicle dynamics in the vicinity of the immune synapse. This technique allows real-time visualization of vesicles within 200 nm of the immune synapse (Campi et al., 2005; Douglass and Vale, 2005; Yokosuka et al., 2005). Transfection of CTLs with VAMP8-TFP showed rapid movement and subsequent accumulation of VAMP8-carrying vesicles in the TIRF plane (Video 1). To simultaneously monitor the dynamics of VAMP8 and recycling endosomes, CTLs were cotransfected with VAMP8-TFP and Rab11a-mCherry and allowed to form synapses with anti-CD3 and anti-CD28 antibody-coated coverslips. Shortly after sedimentation, the appearance and subsequent accumulation of both VAMP8- and Rab11a-containing vesicles could be observed at the immune synapse in the TIRF plane (Fig. 4 A and Video 2). VAMP8-TFP and Rab11a-mCherry exhibited a striking colocalization in the TIRF plane (Fig. 4 A). In comparing the dwell times at the immune synapse, we found that there was no statistically significant difference between Rab11a-mCherry vesicles and VAMP8-TFP vesicles, with VAMP8 dwell time of 14.5 ± 0.7 s compared with 15.7 ± 0.9 s of Rab11a (Fig. 4 B). When we examined vesicle accumulation over time, we also found similar numbers of VAMP8 and Rab11a vesicles at immune synapses (Fig. 4 C).

Interestingly, several rapid fluorescence dispersion events, characteristic of vesicle fusion, were also observed in the TIRF plane (Video 2). Such events were defined as a sudden reduction in fluorescence within 400 ms (i.e., four images), which could be distinguished from movement of granules back into the cell (undocking) that typically lasted >1 s (see Materials and methods for analysis details). Cells exhibited a similar

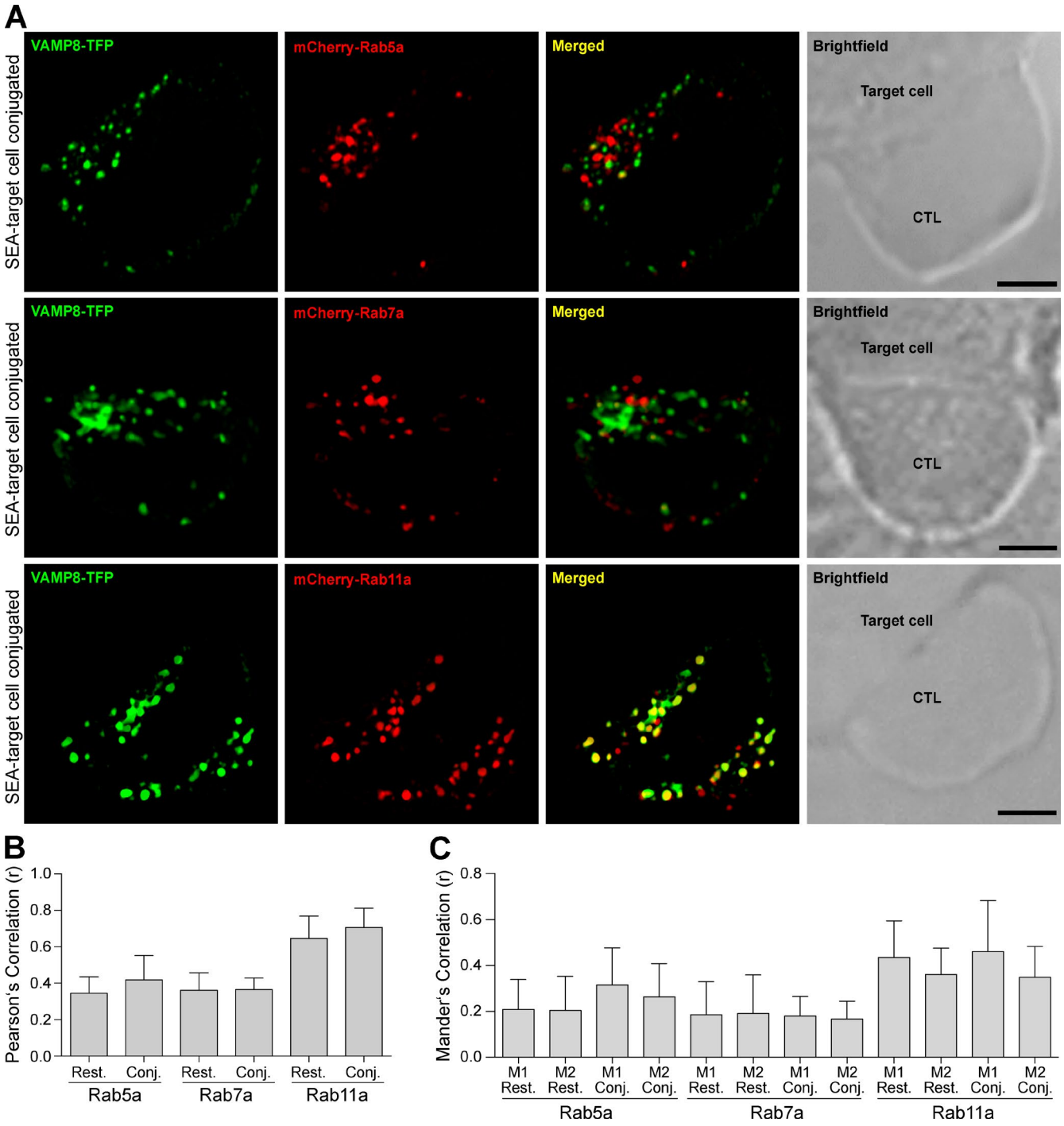

Figure 3. **Vesicular VAMP8 colocalizes with Rab11a.** (A) SIM images of ectopically expressed VAMP8-TFP and mCherry-Rab5a, mCherry-Rab7a, or mCherry-Rab11a localization in unconjugated (top) and SEA-target cell-conjugated (bottom) CTLs as indicated. Bars, 2.5 µm. (B) Pearson's coefficients for VAMP8 and markers of the various endosomal compartments (n = 11, 11, and 12 CTLs, respectively). (C) Mander's coefficients between VAMP8 (M1) and markers of the various endosomal compartments (M2; n = 11). Error bars are means and SDs. Rest., resting; Conj., conjugated.

number of such fusion-like events for both VAMP8-TFP and Rab11a-mCherry (46.9 ± 6.4 vs. 54.0 ± 8.1; Fig. 4 D). Quantification of the cumulative data revealed that rapid fluorescence dispersion events occurred promptly after immune synapse formation (Fig. 4 E). Together, the concerted appearance and fusion-like events, characterized by the quickly forming lateral diffusion clouds, of VAMP8-TFP and Rab11a-mCherry seen in our live imaging (Video 2), clearly indicated that VAMP8 and Rab11a traffic in the same vesicle that may fuse with the plasma membrane subsequently.

To formally demonstrate fusion of VAMP8-carrying recycling endosomes with the plasma membrane, we transfected CTLs with a construct encoding VAMP8 tagged with C-terminal, lumenal 3×FLAG and TFP. Upon fusion of VAMP8-carrying vesicles, the FLAG-tag will be exposed to the extracellular milieu. Addition of the anti-FLAG antibody to the extracellular

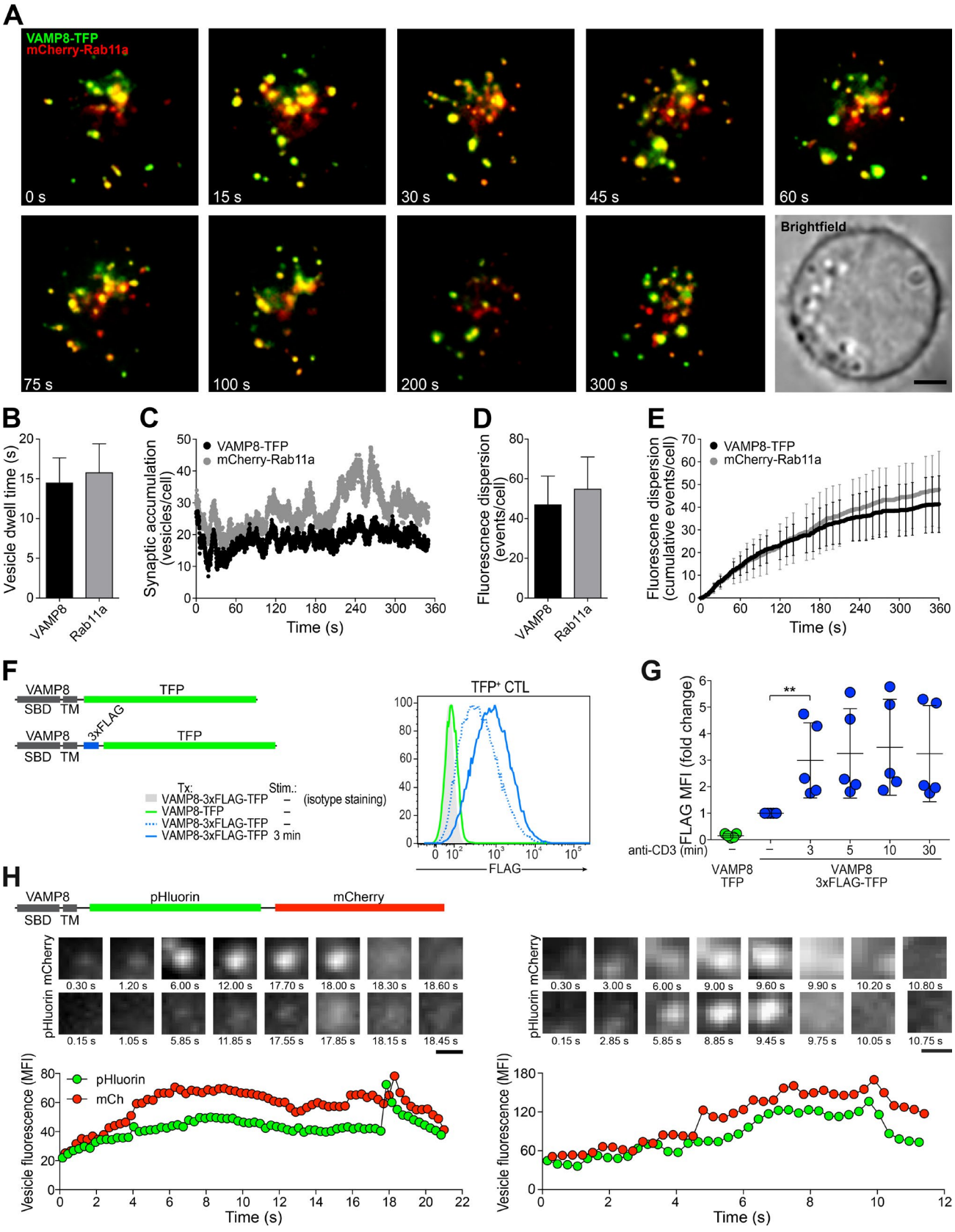

Figure 4. **VAMP8-carrying recycling endosomes accumulate and fuse at immune synapses.** (A–E) Bead-stimulated human CD8+ T cells were transfected with VAMP8-TFP and mCherry-Rab11a encoding constructs and imaged 24 h after transfection. (A) Selected live-cell TIRF microscopy images of VAMP8-TFP and mCherry-Rab11a in a transfected CTL in contact with an anti-CD3– and anti-CD28–coated coverslip. Bar, 2.5 µm. (B) Mean dwell time of VAMP8-TFP and mCherry-Rab11a vesicles in the TIRF plane per cell (n = 15, paired t test, $P > 0.05$). (C) Mean VAMP8-TFP and mCherry-Rab11a vesicle accumulation over time in the TIRF plane per cell (n = 15). (D) Mean fluorescence dispersion events for VAMP8-TFP and mCherry-Rab11a vesicles in the TIRF plane per

milieu followed by flow cytometry and gating on TFP-expressing cells revealed some constitutive expression of VAMP8 on the plasma membrane (Fig. 4, F and G). Upon stimulation with anti-CD3 antibodies, VAMP8 expression on the plasma membrane rapidly increased threefold. Furthermore, to study the characteristics of individual recycling endosome fusion events, CTLs were transfected with a construct encoding VAMP8 tagged with C-terminal, lumenal pHluorin and mCherry (Fig. 4 H). pHluorin is a pH-sensitive variant of GFP that has been used to study vesicle fusion of VAMP2-carrying vesicles in neuronal and endocrine cells (Miesenböck et al., 1998). Transfected cells were imaged by TIRF microscopy. Some vesicles first docked at the immune synapse before undergoing rapid fusion and dispersion of VAMP8 and pHluorin signal (Fig. 4 H, left; and Video 3). In contrast, many vesicles fused immediately after reaching the plasma membrane, sometimes with pHluorin signals remaining clustered before dispersion (Fig. 4 H, right; Fig. S3; and Video 3). Altogether, these results demonstrate that numerous VAMP8-carrying recycling endosomes are rapidly recruited to and fuse with the plasma membrane at CTL immune synapses.

VAMP8-containing recycling endosome fusion precedes perforin-containing cytotoxic granule fusion

To gain further insights to the relationship between VAMP8-carrying recycling endosome activity and cytotoxic granule exocytosis at human immune synapses, CTLs were cotransfected with VAMP8-TFP and perforin-mCherry and allowed to form a synapse with anti-CD3 and anti-CD28 antibody-coated coverslips. CTLs were imaged in real-time by TIRF microscopy. Interestingly, in live-cell imaging, multiple VAMP8-carrying recycling endosomes rapidly appeared in the TIRF plane followed by fewer perforin-containing vesicles (Fig. 5 A and Video 4). Comparing the dwell times of both VAMP8 and perforin vesicles in the TIRF plane, the former resided significantly shorter than the latter (14.5 ± 0.8 s for VAMP8-carrying vesicles vs. 117.4 ± 18.9 s for perforin-containing vesicles, respectively; Fig. 5 B). The accumulation of VAMP8-carrying recycling endosomes outnumbered that of perforin-containing cytotoxic granules at the immune synapse (Fig. 5 C). At the start of the 6-min recording, VAMP8-carrying vesicles showed rapid accumulation that subsided with time. By comparison, perforin-containing vesicles appeared later in the TIRF plane. Comparing fusion-like events revealed by imaging of VAMP8-TFP and perforin-mCherry, CTLs exhibited many more VAMP8 versus perforin fusion-like events per cell (41.6 ± 7.6 vs. 2.4 ± 0.1, respectively; Fig. 5 D). As previously noted, the VAMP8-carrying vesicle fusion-like events occurred promptly after immune synapse formation and then gradually subsided with time (Fig. 5 E). Similar results were also found upon cotransfection of CTL with VAMP8-TFP and granzyme B–mCherry (Fig. S4 and Video 5). In summary, VAMP8-carrying recycling endosome fusion preceded cytotoxic granule exocytosis, implying that recycling endosome fusion with the plasma membrane might be VAMP8 dependent and represent a prerequisite for cytotoxic granule exocytosis.

VAMP8 knockdown ablates recycling endosome and subsequent cytotoxic granule fusion

To determine whether VAMP8 regulates human CTL vesicle exocytosis, we attempted to knockdown the expression of VAMP8 by transfection of CTL with four *VAMP8*-specific siRNAs. Western blot and densitometric analyses showed that VAMP8 expression was reduced by all siRNAs (Fig. 6, A and B). siVAMP8#2 consistently provided the strongest knockdown of VAMP8 expression (with a knockdown efficiency of 70.8 ± 12.6). Staining of transfected cells with a VAMP8-specific antibody confirmed that the expression of VAMP8 was uniformly reduced in CTLs (Fig. S5, A and B). siVAMP8#2 was therefore used for all the following experiments.

To test the involvement of VAMP8 in recycling endosome fusion, we performed TIRF microscopy of CTLs cotransfected with Rab11a-mCherry and control siRNA or VAMP8 siRNA. Knockdown of VAMP8 did not significantly change the mean dwell time of Rab11a-carrying vesicles (17.8 ± 0.5 vs. 21.1 ± 2.4; Fig. 6 C). However, in contrast to cells transfected with control siRNA, VAMP8 siRNA-transfected cells showed a very strong reduction of Rab11a fusion-like events (42.4 ± 5.3 vs. 8.3 ± 1.9; Fig. 6 D and Video 6). Consequently, our results indicate that VAMP8 is a vesicular SNARE required for fusion of recycling endosomes with the plasma membrane.

Studies of knockout mice have implicated VAMP8 in many forms of secretory granule secretion (Paumet et al., 2000; Wang et al., 2004; Ren et al., 2007; Loo et al., 2009; Dressel et al., 2010). Despite not being localized to cytotoxic granules in human CTL, we examined whether siRNA-mediated VAMP8 knockdown would affect cytotoxic granule exocytosis. First, we performed TIRF microscopy on CTL transfected with VAMP8 siRNA and the cytotoxic granule marker granzyme B–mCherry to visualize cytotoxic granule trafficking and fusion. After sedimentation of CTLs, cytotoxic granules could be observed fusing at the immune synapse in the TIRF plane (Fig. 6 E and Video 7). Knockdown of VAMP8 did not significantly change the mean dwell time of granzyme B–containing vesicles (Fig. 6 F). In contrast to cells transfected with control siRNA, VAMP8 siRNA–transfected cells showed a strong reduction (>87%) in granzyme B–mCherry fusion-like events (Fig. 6 G and Video 7). Moreover, VAMP8 knockdown also reduced degranulation as measured by induced surface expression of CD107a (also known as lysosome-associated membrane protein 1 [LAMP-1]; Fig. 6, H and I). These experiments revealed that VAMP8

cell (n = 16, paired t test, $P > 0.05$). (E) Mean cumulative fluorescence dispersion events for VAMP8-TFP and mCherry-Rab11a vesicles in the TIRF plane per cell (n = 15). (F and G) Bead-stimulated human CD8$^+$ T cells were transfected with constructs encoding VAMP8-TFP or VAMP8-3×FLAG-TFP and analyzed by flow cytometry 24 h after transfection. CTLs were stimulated with anti-CD3 and anti-CD28 antibodies and then surface stained with the anti-FLAG antibody. (F) Schematic representations of the constructs indicating the SNARE domain (SD) and transmembrane (TM) domains are depicted. Histograms from one representative donor show FLAG staining on TFP$^+$ CTL, as indicated. Data are representative of three independent experiments performed on multiple donors. SBD, syntaxin binding domain. (G) Graphs depict FLAG mean fluorescent intensity (MFI) relative to unstimulated, VAMP8-3×FLAG-TFP–transfected CTLs in five individual donors. Mean and SDs are indicated (paired t test, **, $P < 0.01$). (H) Bead-stimulated human CD8$^+$ T cells were transfected with VAMP8-pHluorin-mCherry (mCh) encoding constructs and imaged 24 h after transfection. Selected live-cell TIRF microscopy frames of two individual CTL vesicles are shown, as indicated. Graphs below depict respective pHluorin and mCherry vesicle MFI over time (experiments were repeated with three individual donors and n = 10 cells). Bars, 0.15 µm. Error bars show means and SDs.

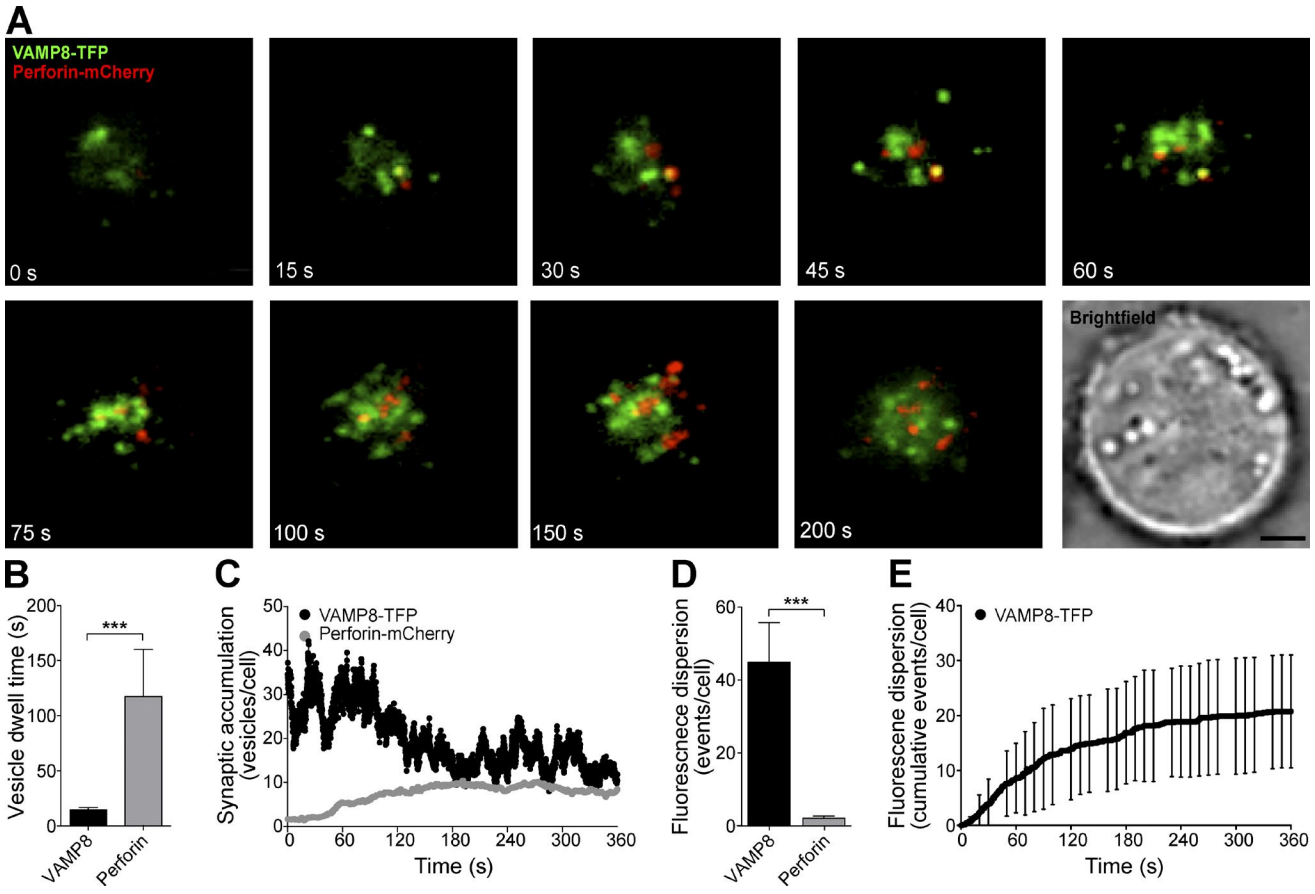

Figure 5. **VAMP8-carrying cells accumulate and fuse at the immune synapse before cytotoxic granules.** (A–E) Bead-stimulated human CD8+ T cells were transfected with VAMP8-TFP and perforin-mCherry encoding constructs and imaged 24 h after transfection. (A) Selected live-cell TIRF microscopy images of VAMP8-TFP and perforin-mCherry in a transfected CTLs in contact with an anti-CD3– and anti-CD28–coated coverslip. Bar, 2.5 µm. (B) Mean dwell time of VAMP8-TFP and perforin-mCherry vesicles in the TIRF plane per cell (n = 15, paired t test, ***, P > 0.001). (C) Mean VAMP8-TFP and perforin-mCherry vesicle accumulation over time in the TIRF plane per cell (n = 15). (D) Mean fluorescence dispersion events for VAMP8-TFP and perforin-mCherry vesicles in the TIRF plane per cell (n = 15, paired t test, ***, P > 0.001). (E) Cumulative fluorescence dispersion events for VAMP8-TFP and perforin-mCherry vesicles in the TIRF plane per cell (n = 18). Error bars show means and SDs.

is required for both recycling endosome and cytotoxic granule fusion with the plasma membrane. Although our results suggested that VAMP8 is required for an early fusion event obligatory to cytotoxic granule exocytosis, it was not clear whether VAMP8-mediated fusion of recycling endosomes with the plasma membrane is required for TCR signaling and immune synapse formation or, further downstream and more specifically, the assembly of the plasma membrane SNARE complex for cytotoxic granule fusion.

VAMP8 regulates Stx11 deposition at immune synapses but not proximal TCR signaling

To further dissect the mechanism whereby VAMP8 facilitates lymphocyte cytotoxicity, we first studied the impact of VAMP8 knockdown on TCR signaling in human CTLs. CTLs were transfected with control siRNA or VAMP8 siRNA, labeled with Fluo-4 and Fura red Ca^{2+}-sensitive dyes, and assessed by ratiometric flow cytometry. Knockdown of VAMP8 did not significantly alter intracellular Ca^{2+} mobilization after TCR stimulation (Figs. 7 A and S5 D), which is crucial for lymphocyte cytotoxicity (Maul-Pavicic et al., 2011). Similarly, knockdown of VAMP8 did not reduce phosphorylation of the MAPK extracellular signal–regulated kinase (ERK) after TCR stimulation (Fig. 7, B and C; and Fig. S5 E). ERK phosphorylation has been implicated in cytotoxic lymphocyte granule polarization (Jenkins et al., 2009). Thus, VAMP8 was not required for proximal TCR signals leading to intracellular Ca^{2+} mobilization and phosphorylation of ERK. To study actin dynamics, CTLs were cotransfected with recombinant, fluorescently tagged actin (LifeAct-GFP) and control siRNA or VAMP8 siRNA and subsequently imaged by TIRF microscopy (Fig. 7, D and E; and Fig. S5 F). In line with the experiments negating a role for VAMP8 in proximal TCR-induced Ca^{2+} mobilization and phosphorylation of ERK, knockdown of VAMP8 did not affect established F-actin architectural phases during immune synapse formation (Rak et al., 2011). An even distribution of F-actin was initially observed upon contact with the coverslip. After cell spreading and within ∼40 s, distribution of F-actin around the cell perimeter was observed. This annular distribution was accompanied by the appearance of granule-sized clearance in the actin meshwork and normal cell spreading (Fig. 7, E and F). In conclusion, our results indicated that VAMP8-mediated fusion with the plasma membrane is not required for proximal TCR-induced signaling and actin reorganization.

We have recently shown that Stx11 localizes to recycling endosomes in human CTLs (Halimani et al., 2014). We therefore postulated that knockdown of VAMP8 might change Stx11

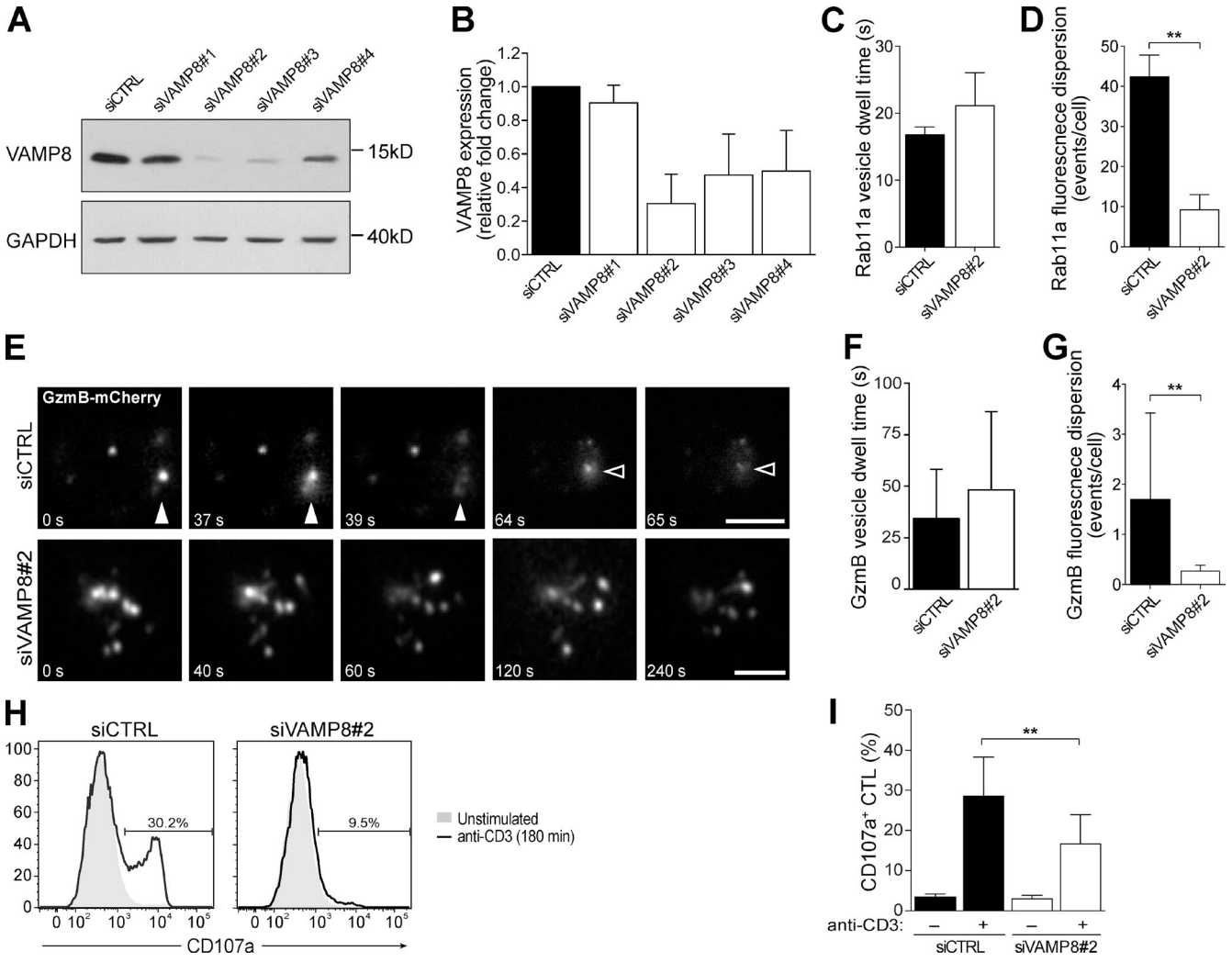

Figure 6. **VAMP8 is required for fusion of recycling endosomes and cytotoxic granules at the immune synapse.** (A and B) Bead-stimulated human CD8+ T cells were transfected with siRNA, as indicated. VAMP8 expression was determined by Western blot analysis. (A) Expression of VAMP8 relative to GAPDH in transfected CTLs, as indicated, from one representative donor. (B) Graphs represent means, normalized expression of VAMP8 in transfected CTLs, as indicated, from four individuals. Bars indicate SDs. (C–G) Bead-stimulated human CD8+ T cells were transfected with control siRNA or siVAMP8#2 siRNA, as indicated, and mCherry-Rab11a (C and D) or granzyme B (GzmB)–mCherry (E–G) encoding constructs and imaged by TIRF microscopy on anti-CD3– and anti-CD28–coated coverslips 16–20 h after transfection. (C) Mean dwell time of mCherry-Rab11a vesicles in the TIRF plane per cell (n = 15). (D) Mean fluorescence dispersion events for mCherry-Rab11a vesicles in the TIRF plane per cell (n = 15, unpaired t test, **, P > 0.01). (E) Selected live-cell TIRF microscopy images of granzyme B–mCherry in representative CTLs transfected with siRNA as indicated. Fusion event are indicated with arrowheads; vesicle 1 is indicated by closed arrowheads, and vesicle 2 is indicated by open arrowheads. Bars, 5 µm. (F) Mean dwell time of granzyme B–mCherry vesicles in the TIRF plane per cell (n = 8). Error bars indicate SDs. (G) Mean fluorescence dispersion events for granzyme B–mCherry vesicles in the TIRF plane per cell (n = 15, unpaired t test, **, P > 0.01). Error bars indicate SDs. (H and I) Bead-stimulated human CD8+ T cells were transfected with siRNA, as indicated, and analyzed by flow cytometry 18 h after transfection. CTLs were stimulated with anti-CD3 and anti-CD28 antibodies and then surface stained with the anti-CD107a antibody. (H) Representative histograms of CD107a staining on gated CTLs, as indicated, experiments were repeated with six individual donors, and data are quantified in I. CD8+ cells were isolated and stimulated with CD3/CD28 beads for 48 h and then transfected with control or VAMP8 siRNA. After 18 h, the cells were supplemented with anti-CD3 antibody for 3 h. After stimulation, the lymphocytes were surface stained for CD107 expression. Percentages indicate the increase in CD107 expression on the cell surface compared to nonstimulated conditions. (I) Graphs depict the mean frequency of CTLs, transfected and stimulated as indicated, expressing surface CD107a in six individual donors (ANOVA, **, P > 0.01). Error bars indicate SDs. siCTRL, control siRNA.

dynamics and interfere with downstream cytotoxic granule exocytosis. To test this hypothesis, CTLs were cotransfected with Stx11-mCherry and control siRNA or VAMP8 siRNA. CTLs were subsequently imaged using TIRF microscopy (Figs. 7 G and S5 G and Video 8). Knockdown of VAMP8 led to an increase in dwell time of Stx11-carrying vesicles (Fig. 7 H). Paralleling this, knockdown of VAMP8 led to a cumulative increase in the number of Stx11-carrying vesicles as well as the overall Stx11 fluorescence intensity in the TIRF plane (Fig. 7, I and J). Remarkably, Stx11 vesicle fluorescence dispersion events were greatly reduced in VAMP8 knockdown compared with control CTLs (10 ± 3.9 vs. 1.3 ± 1.26, respectively; Fig. 7 K). VAMP8 and, even more so, Stx11 fluorescence dispersion events were predominately focused toward the center of the immune synapse (Fig. 7, L–N) suggesting a degree of recycling endosome exocytosis polarization. With respect to the radial distribution of Stx11, VAMP8 knockdown resulted in an increased central clustering of Stx11-carrying vesicles at the immune synapse (Fig. 7 O), possibly reflecting a microtubule-organizing complex–coordinated polarization of recycling endosomes toward

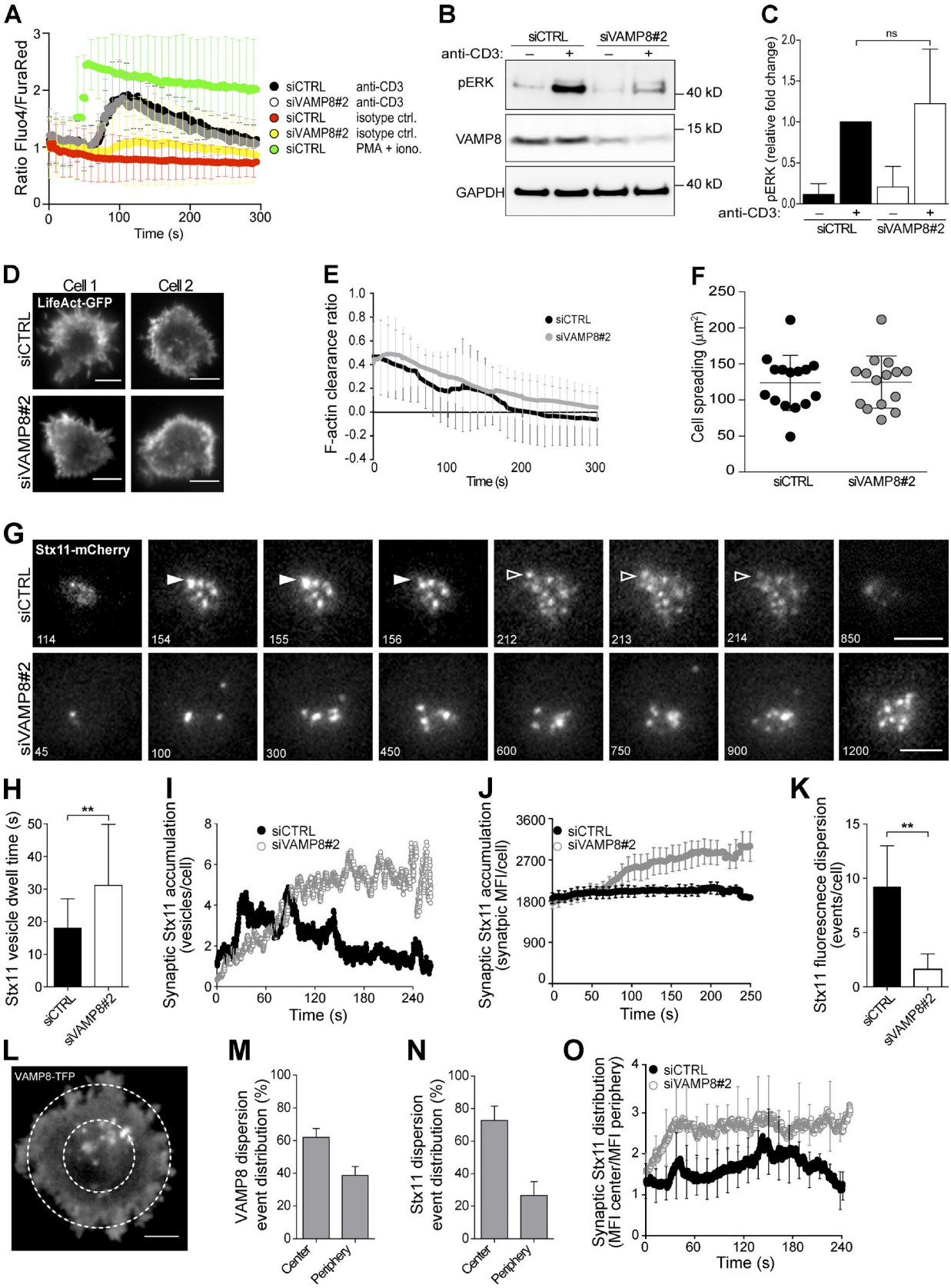

Figure 7. **VAMP8 knockdown does not affect proximal T cell signaling, but regulates Stx11 vesicle trafficking and fusion at immune synapses.** (A–K) Bead-stimulated human CD8+ T cells were transfected with siRNA, as indicated, as well as LifeAct-GFP (D–F) or Stx11-mCherry (G–K). (A) CTLs were loaded with Ca^{2+}-sensitive Fluo-4 and Fura red dyes and assessed by flow cytometry and stimulated as indicated. iono., ionomycin. (B and C) Western blot of CTL lysates after transfection and stimulation as indicated. (B) Blots for phospho-ERK (pT202/pY204), VAMP8, and loading control GAPDH are shown for one representative donor. (C) Densitometry analysis of phospho-ERK signaling in five individual donors. Mean values are indicated, with bars representing

the immune synapse. With VAMP8 knockdown, Stx11 deposition and diffusion in the membrane would be reduced, resulting in an increased central clustering of Stx11. Hence, our results suggest that Stx11 deposition into the plasma membrane is specifically mediated by VAMP8 recycling endosome fusion.

Discussion

The mechanisms of lymphocyte cytotoxicity have not been fully elucidated (de Saint Basile et al., 2010). In studying the R-SNARE candidate VAMP8, we made several unexpected discoveries. Super high resolution imaging of both endogenous and ectopically expressed VAMP8 in primary human CTLs established that VAMP8 localizes to the Rab11a-positive recycling endosome compartment rather than to cytotoxic granules. Complimentary approaches demonstrated that VAMP8-carrying recycling endosomes rapidly fuse with the plasma membrane upon TCR engagement of CTLs. Moreover, VAMP8 knockdown demonstrated a critical role for VAMP8 in fusion of recycling endosomes with the plasma membrane at immune synapses. In agreement with previous studies of *Vamp8* knockout mice (Loo et al., 2009; Dressel et al., 2010), VAMP8 knockdown also impaired cytotoxic granule exocytosis by human CTLs. Intriguingly, we found that VAMP8 knockdown did not diminish proximal TCR signaling, implying that VAMP8-mediated fusion plays a more specific role in promoting cytotoxic granule exocytosis. Our data suggest that VAMP8-dependent recycling endosome fusion deposits the Qa-SNARE Stx11, localized to recycling endosomes in unstimulated CTL (Halimani et al., 2014), on the plasma membrane at immune synapses for cytotoxic granule exocytosis.

CTLs survey tissues for aberrant cells and can engage and kill target cells within 2 min through regulated exocytosis of specialized secretory lysosomes (Lopez et al., 2013). Exocytosis of cytotoxic proteins needs to be stringently controlled. Remarkably, we found accumulation and exocytosis of numerous VAMP8-carrying, Rab11-positive recycling endosomes within seconds of CTL contact with anti-CD3–coated coverslips. The exocytosis of these vesicles not only outnumbered but also preceded that of perforin- and granzyme B–containing cytotoxic granules. On average, 40 or more recycling endosomes fused with the plasma membrane within 4 min of CTL immune synapse formation. By comparison, less than five fusion-like events of cytotoxic granules were observed per cell. Recycling endosomes have previously been implicated in SNARE-dependent accumulation of TCR clusters to the immune synapse (Das et al., 2004). Specifically, synaptotagmin 7 and VAMP7 mediate fusion of vesicles containing TCR and LAT, respectively (Larghi et al., 2013; Soares et al., 2013). TCR-induced signaling is impaired in VAMP7-deficient $CD4^+$ T cells (Larghi et al., 2013). Whether these vesicles fuse with the plasma membrane or form intracellular signaling platforms is disputed. Our data suggest that VAMP8 mediates recycling endosome fusion with the plasma membrane for delivery of molecules required for cytotoxic granule exocytosis but is not crucial for T cell activation. There is quite possibly heterogeneity in the lymphocyte recycling endosome compartment, where different vesicles may contribute to intracellular signaling versus delivery of cargo to the plasma membrane. Importantly, we find that VAMP8 is required for deposition of Stx11, an effector molecule of cytotoxic granule fusion (Bryceson et al., 2007), at the immune synapse. Thus, we posit a two-step sequential process for lymphocyte cytotoxicity in which VAMP8-mediated recycling endosome fusion brings effector proteins to the plasma membrane for SNARE complex formation and subsequent cytotoxic granule exocytosis (Fig. 8). Our data suggest that recycling endosome fusion is clustered toward the center of the immune synapse, possibly reflecting involvement of the microtubule-organizing complex in both recycling endosome and cytotoxic granule exocytosis. It is possible that additional engagement of integrins at cytotoxic immune synapses would further promote polarization of the recycling endosome compartment to a focal site of exocytosis (Stinchcombe et al., 2006; Liu et al., 2009). Moreover, although our data suggest recycling endosome fusion is critical for delivery of Stx11 to the immune synapse, it is also possible that VAMP8-mediated recycling endosome fusion with the plasma membrane provides other proteins required for cytotoxic granule exocytosis. It is worth noting that Munc13-4 also resides on Rab11-positive recycling endosomes (Ménager et al., 2007). Besides mediating cytotoxic granule to plasma membrane fusion, Munc13-4 has been previously proposed to promote late endosome to lysosome fusion, facilitating cytotoxic granule maturation (Ménager et al., 2007). It will therefore be interesting to address how distinct Munc13-4 isoforms may be involved in regulating exocytosis of recycling endosomes and cytotoxic granules (Cichocki et al., 2014). In summary, our findings unravel a novel component of vesicular fusion for lymphocyte cytotoxicity, providing a new layer of control in the carefully orchestrated process of target cell killing.

Several genes required for cytotoxic granule exocytosis have been linked to development of early onset, often fatal hyperinflammatory syndromes such as HLH. Loss-of-function mutations in *VAMP8* have so far not been associated with HLH. The very small coding region of *VAMP8* may explain why deficiencies in VAMP8 are exceedingly rare, and patients have not been described to date. Alternatively, VAMP8 deficiency may lead to a disparate clinical presentation. Notably, one third of *Vamp8* knockout mice die before the age of 1 mo (Wang et al., 2004; Kanwar et al., 2008). By comparison, *Prf1* knockout mice

SDs (ANOVA). (D) TIRF microscopy images of CTLs transfected with siRNA, as indicated, and LifeAct-GFP after contact with anti-CD3 and anti-CD28 antibody-coated coverslips for 250 s. (E) Quantification of F-actin clearance based on LifeAct-GFP fluorescence in individual cells (n = 12). (F) Quantification of cell spreading was based on LifeAct-GFP fluorescence in individual cells (n = 15). (G) Selected live-cell TIRF microscopy images of mCherry-Stx11 in representative CTLs transfected with siRNA as indicated. Arrowheads indicate fusion events; vesicle 1 is indicated by closed arrowheads, and vesicle 2 is indicated by open arrowheads. (H) Mean dwell time of mCherry-Stx11 vesicles in the TIRF plane per cell (n = 15, unpaired t test, **, P > 0.01). (I) Mean mCherry-Stx11 vesicle accumulation over time in the TIRF plane per cell (n = 20). (J) Mean overall mCherry-Stx11 accumulation over time in the TIRF plane per cell (n = 20). (K) Mean fluorescence dispersion events for mCherry-Stx11 vesicles in the TIRF plane per cell (n = 15, unpaired t test, **, P > 0.01). (L) Representative TIRF image depicting concentric circle region of interest used for radial analysis and dispersion of VAMP8-TFP and mCherry-Stx11. (M) Graph depicts the distribution of cumulative VAMP8-TFP fluorescence dispersion events on a per cell basis. (N) Graph depicts the distribution of cumulative mCherry-Stx11 fluorescence dispersion events on a per cell basis. (O) Quantification of mCherry-Stx11 radial distribution in TIRF plane of CTLs cotransfected with siRNA, as indicated. siCTRL, control siRNA. Bars: (D and G) 5 µm; (L) 2.5 µm.

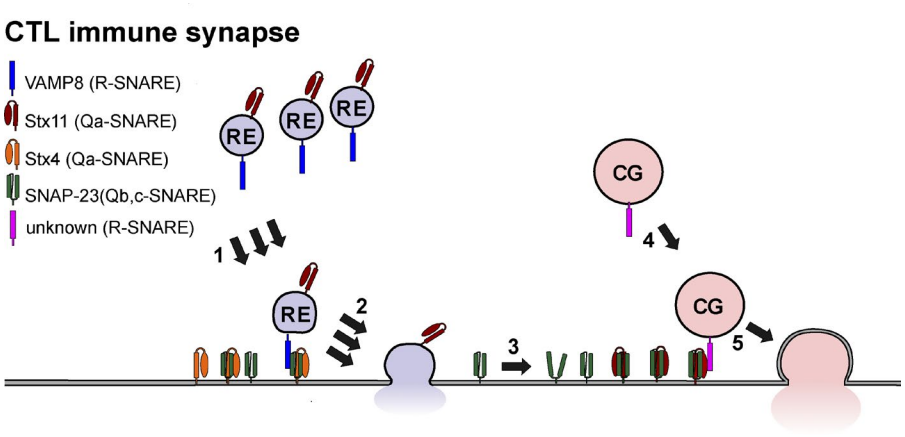

Figure 8. **Proposed sequential model for cytotoxic lymphocyte exocytosis.** (A) After target cell recognition, numerous small recycling endosomes (RE) carrying VAMP8 and Stx11 (1) traffic to the CTL immune synapse and (2) undergo VAMP8-dependent fusion with the plasma membrane, possibly through interaction with plasma membrane Stx4 and SNAP-23 SNARE complex partners. Such exocytosis of recycling endosomes deposits high amounts of Stx11 molecules in the plasma membrane, which may (3) lead to the formation of Stx11 and SNAP-23 SNARE complexes. Initial activity at the immune synapse thus forms "active zones" where (4) docking through interactions of R-SNARE proteins on larger cytotoxic granules (CGs) with plasma membrane Stx11–SNAP-23 complexes can facilitate (5) cytotoxic granule exocytosis that releases cargo necessary for target cell killing.

are healthy until challenged by viral infection (Kägi et al., 1994), suggesting that VAMP8 mediates vital physiological functions in addition to lymphocyte cytotoxicity. Such functions may include pancreatic secretion. Thus, VAMP8 deficiency in humans may give rise to a distinct phenotype or be embryonically lethal.

VAMP8 was originally identified as a widely expressed R-SNARE predominantly localized to the early endocytic pathway (Wong et al., 1998). Blocking studies in cell lines using antisera suggest that VAMP8 mediated homotypic fusion of early as well as late endosomes (Antonin et al., 2000b). Although VAMP8 has not been previously linked to recycling endosome fusion with the plasma membrane, several recent studies have implicated VAMP8 in secretory exocytic pathways of various cell types. In the pancreas, VAMP8 facilitates release of zymogen from acinar cells secretory granules by forming a SNARE complex with Qa-SNARE Stx4 and the Qb/Qc-SNARE SNAP-23 (Wang et al., 2004). Studies of knockout mice have revealed that VAMP8, but not VAMP2 or VAMP3, is required for secretory granule exocytosis in platelets (Ren et al., 2007). Similarly, studies of human and mouse mast cells have shown that VAMP8 mediates release of serotonin from lysosomal secretory granules (Puri and Roche, 2008; Sander et al., 2008). However, these studies did not establish the localization or trafficking of VAMP8 by high-resolution microscopy. Our data investigating the subcellular localization of endogenous, as well as ectopically expressed VAMP8, in CTLs clearly established localization of VAMP8 to a subset of Rab11a-positive recycling endosomes. Moreover, using luminal tags or pH-sensitive probes, we demonstrated that VAMP8-carrying vesicles undergo fusion with the plasma membrane at immune synapses before secretory/cytotoxic granule exocytosis. In light of our novel insights into the vesicle fusion processes regulating lymphocyte cytotoxicity, dissections of VAMP8-dependent secretory granule exocytosis pathways in other cell types using high-resolution imaging are warranted. It is an intriguing possibility that VAMP8-mediated recycling endosome fusion may also represent a previously unrecognized step in the release of secretory granule contents by these other cell types, potentially revealing additional layers of complexity to their exocytic pathways.

The identity of other components of the SNARE complex mediating recycling endosome fusion in CTLs is not clear. VAMP8 can form a complex with Stx7, Stx8, and Vti1b for late endosome to lysosome fusion (Antonin et al., 2000a). In primary human CTLs, Stx4 localizes to the plasma membrane and accumulates at the immune synapse (Pattu et al., 2012), making it a strong SNARE candidate for the recycling endosome fusion. Preliminary immunoprecipitation experiments in our laboratory indicated that VAMP8 also interacts with Stx4 in CTL but failed to show any interaction with Stx7 or Stx8 (unpublished data). Additional experiments are required to verify the identity and spatiotemporal dynamics of the other SNARE complex partners, mediating recycling endosome to plasma membrane fusion in lymphocytes.

In conclusion, our findings reveal a role for VAMP8 in fusion of recycling endosomes with the plasma membrane. In CTLs, our data demonstrate that VAMP8-dependent recycling endosome fusion mediates plasma membrane delivery of proteins, i.e., Stx11, specifically required for cytotoxic granule exocytosis. Our data provide a new mechanistic view of cytotoxic lymphocyte exocytosis. In conjunction with the literature on VAMP8, our findings may warrant further high-resolution functional dissection of exocytosis in other cell types in which VAMP8 has been implicated in release of secretory granule content.

Materials and methods

Cells

Research with human material performed for this study has been approved by the local ethics committee. Human peripheral blood mononuclear cells (PBMCs) were isolated from healthy donors by density gradient centrifugation (Lymphoprep; Axis-Shield). In some experiments, PBMCs were stimulated with 5 µg/ml of SEA at a density of 10^8 cells/ml at 37°C for 1 h. Stimulated PBMCs were thereafter resuspended at a density of 1.5×10^6 cells/ml in complete medium (AIM V medium; Invitrogen) supplemented with 10% FCS (Invitrogen) and 2% human AB sera (Sigma-Aldrich) supplemented with 100 IU/ml of recombinant human IL-2 (Biosource). After 5 d, SEA-specific CTLs were positively selected (Dynal $CD8^+$ isolation kit; Invitrogen) and cultured further in complete medium. CTLs from day 2–3 after positive isolation were used for experiments. For bead-stimulated CTLs, $CD8^+$ T cells were isolated from PBMCs by negative magnetic selection ($CD8^+$ negative isolation kit; Invitrogen) and stimulated with antibody-coated beads (Dynabeads Human T-Activator CD3/CD28; Invitrogen) in complete medium.

Antibodies

For Western blotting, rabbit polyclonal anti-VAMP8 (V7389; Sigma-Aldrich), anti-phospho-p42/44 MAPK (Erk1/2, Thr202/Tyr204; 9101;

Cell Signaling Technology), and anti-GAPDH (Cell Signaling Technology) antibodies were used. Secondary antibodies were HRP-conjugated donkey anti–rabbit (Invitrogen). For confocal microscopy, mouse monoclonal anti-perforin (δG9; BioLegend) and anti–granzyme B (GB11; BioLegend) as well as rabbit polyclonal anti-VAMP8 (W. Hong) antibodies were used. The VAMP8 antibody was generated using residues 1–75 of VAMP8, expressed as a fusion protein to GST (GST-endobrevin) and used to raise polyclonal antibodies against endobrevin. For TIRF microscopy and flow cytometric assays, mouse anti–human monoclonal anti-CD3 (BB11; Euroclone), mouse anti–human CD28 (CD28.2; BD), and mouse anti–human isotype IgG1 (MOPC-21; BD) antibodies were used for coating coverslips and stimulating cells. For flow cytometry stainings, fluorochrome-conjugated mouse anti–human monoclonal antibodies were used as follows: anti-CD3 (S4.1; Invitrogen), anti-CD4 (S3.5; Invitrogen), anti-CD8 (3B5; Invitrogen), anti-CD107a (H4A3; BD), and anti-FLAG (M2; GenScript).

Plasmids

The *VAMP8* coding sequence was amplified from human cDNA with forward primer 5′-TATAGAATTCCACCATGGAGGAAGCCAGTGAAG-3′ and reverse primer 5′-TATAGGTACCTTAAGAGAAGGCACCAGTGGCAA-3′ and inserted in frame with C-terminal TFP and mCherry in a pC1-EGFP (Takara Bio Inc.) derived vector which has a cytomegalovirus (CMV) promoter (Pattu et al., 2011). mCherry-Rab5a, -Rab7a, and -Rab11a constructs have been previously described (Qu et al., 2011), as have the mCherry-perforin, mCherry–granzyme B, and mCherry-Stx11 constructs (Pattu et al., 2011; Matti et al., 2013; Halimani et al., 2014). Vectors coding for pmTFP-C1 and mCherry-C1 under control of a CMV promoter were generated by replacing GFP within pEGFP-C1 (Takara Bio Inc.) with mTFP (Allele Biotech) or mCherry (gift from R. Tsien, New York University Neuroscience Institute, New York, NY), respectively, using AgeI and BglII sites. To generate mCherry-Rab5a, human Rab5a-encoding cDNA was amplified with forward primer 5′-TATATGAATTCTATGGCTAGTCGAGGCGCAA-3′ and reverse primer 5′-TATATAGGATCCTTAGTTACTACAACACTGATTCCTG-3′ and ligated with mCherry-C1 at the N-terminal end of Rab5a. To generate mCherry-Rab7a, human Rab7a-encoding cDNA was amplified with primers 5′-TATATGAATTCTATGACCTCTAGGAAGAAAGTGT-3′ and 5′-TATATAGGATCCTCAGCAACTGCAGCTTTCTG-3′ and ligated with mCherry-C1 at the N-terminal end of Rab7a. To generate mCherry-Rab11a, human Rab11a-encoding cDNA was amplified with primers 5′-TATATGAATTCTATGGGCACCCGCGACGAC-3′ and 5′-TATATAGGATCCTTAGATGTTCTGACAGCACTG-3′ and ligated with mCherry-C1 at the N-terminal end of Rab11a (Qu et al., 2011). Human perforin-encoding cDNA was amplified with primers 5′-TATATAAGATCTCCACCATGGCAGCCCGTGTGCTCC-3′ and 5′-TATATATACCGGTGGCCACACGGCCCCACTCCGG-3′ and ligated with C-terminal mCherry using BglII and AgeI restriction sites. Similarly human granzyme B–encoding cDNA was amplified with primers 5′-TATACTCGAGCCACCATGCAACCAATCCTGCTTCTG-3′ and 5′-ATATATCCGCGGGTAGCGTTTCATGGTTTTCTTT-3′ and ligated with C-terminal TFP or mCherry-encoding sequences. The VAMP8-TFP and VAMP8-mCherry constructs are described further in this section. To generate constructs encoding VAMP8 fused to mCherry and pHluorin, human VAMP8-encoding cDNA was amplified along with a linker sequence onto the PCR product from the VAMP8-TFP construct using the primers 5′-GCAGGTACCGTCACCATGGAGGAAGCCAGTGAAGG-3′ and 5′-GCCAGATCTTTTGTATAGTTCATCCATGCC-3′ and ligated to the pmaxGFP (Miltenyi Biotec) backbone containing mCherry at the C-terminal end of pHluorin. The pHluorin was derived from a pHluorin FasL construct, a gift from E. Long (National Institute of Allergy and Infectious Diseases, National Institutes of Health, Rockville, MD, using primers 5′-GCCACTGGTGCCTTCTCTGCTAGCGGCGGCTCTGGCGGCTCTGGCGGCTCTATGAGTAAAGGAGAAGAACTT-3′ and 5′-GCCAGATCTTTTGTATAGTTCATCCATGCC-3′. VAMP8-3×FLAG-TFP was generated by linearizing VAMP8-TFP with EcoRI and AgeI and inserting a 3×FLAG encoding sequence. The 3×FLAG sequence was generated using overlapping forward and reverse complementary primers, which were annealed to generate 3×FLAG with EcoRI and AgeI using primers 5′-AATTCTGGACTACAAAGACCATGGCGATTATAAAGATCATGACATCGACATCGACTACAAGGATGACGATGACAAGCCA-3′ and 5′-TGGCTTGTCATCGTCATCCTTGTAGTCGATGTCATGATCTTTATAATCGCCATGGTCTTTGTAGTCAG-3′. To generate mCherry-Stx11 or TFP-Stx11, human Stx11-encoding cDNA was amplified with primers 5′-TATAAAGCTTCCATGAAAGACCGGCTAGCAGAA-3′ and 5′-TATAGGATCCCTACTTGAGGCAGGGACAGCA-3′ and ligated with TFP-C1 or mCherry-C1 at the N-terminal end of Stx11 in a pEGFP-C1 (Takara Bio Inc.) vector with a CMV promoter (Pattu et al., 2011; Matti et al., 2013; Halimani et al., 2014). LifeAct was a gift from R. Wedlich-Söldner (Institute of Cell Dynamics and Imaging, University of Münster, Münster, Germany; Riedl et al., 2008).

qRT-PCR

Total RNA was extracted (TRIzol; Invitrogen) and reverse transcribed (SuperScript II; Invitrogen) using random hexamer primers. Quantitative PCR was performed using specific *VAMP8* and *UBC* primers and SYBR green dye (QuantiTect SYBR Green PCR kit; QIAGEN) on a quantitative PCR system (Mx3000P; Agilent Technologies). *VAMP8* primers were forward, 5′-TGATCGTGTGCGGAACCTGCA-3′, and reverse, 5′-GCTCAGATGTGGCTTCCAGATCCT-3′. *UBC* primers were forward, 5′-ATTTGGGTCGCGGTTCTTG-3′, and reverse, 5′-TGCCTTGACATTCTCGATGGT-3′. The data were normalized to *UBC*.

Western blot analysis

Human CTLs were homogenized with a syringe in lysis buffer (50 mM Tris, pH 7.4, 1 mM EDTA, 1% Triton X-100, 150 mM NaCl, 1 mM DTT, 1 mM deoxycholate, protease inhibitors, and PhosSTOP [Roche]) on ice. Lysates were rotated for 30 min at 4°C, and insoluble material was removed by centrifugation at 10,000 RCF. The protein concentration in lysates was determined using Bradford assay (Thermo Fisher Scientific). Proteins were separated by SDS-PAGE (NuPAGE; Invitrogen), transferred to nitrocellulose membranes (Invitrogen), and blocked by incubation with 5% skim milk powder in 20 mM Tris, 0.15 M NaCl, pH 7.4, and TBS for 2 h or overnight and blotted with specific antibodies. Blots were developed using enhanced chemoluminescence reagents (SuperSignal West Dura Chemoluminescent Substrate; Thermo Fisher Scientific) and scanned. For expression analysis, the pixel area and mean fluorescence intensity (MFI) were determined with ImageJ v1.46 (National Institutes of Health). Integrated density was calculated by multiplying band pixel area by the MFI.

Nucleofection of expression constructs and siRNA-mediated knockdown

After 2 d of bead stimulation, 5×10^6 CTLs were transfected with 1.5 µg of plasmid DNA (Human T cell nucleofector kit; Lonza). Cells were imaged 24–30 h after transfection. For knockdown of protein expression, 5×10^6 CTLs were transfected with 2 µM of siRNA (Hs_VAMP8_4 SI02656766 or SI03650325; QIAGEN) using the nucleofector kit (Lonza). After 12 h of incubation, the cells were washed and cultured in AIM V without IL-2 and used for experiments 18 h after transfection. Knockdown efficiency was assessed by preparing whole cell lysates of 10^6 CTLs boiled in SDS loading buffer containing 4% β-mercaptoetha-

nol and 1 mM DTT. Lysates were sonicated, proteins were separated by SDS-PAGE, and expression was analyzed by Western blotting.

SIM

To conjugate CTLs with target cells, Raji cells were pulsed with 10 µg/ml SEA at 37°C for 30 min. The stimulation of Raji cells was performed in 96-well plates with a maximum of one million cells resuspended in 100 µl AIM V medium. The CTL- and SEA-pulsed Raji cells were washed once with AIM V and resuspended at a concentration of 2×10^7 cells/ml. CTLs were mixed with target cells at a 1:1 ratio and left in suspension for 5 min at 37°C. The cell suspension was then diluted to a concentration of 4×10^6 cells/ml with AIM V medium and plated onto poly-ornithine–coated 12-mm glass coverslips and incubated at 37°C for 15 min. Cells were fixed in ice-cold 4% PFA in Dulbecco's PBS (Invitrogen) and stained with antibodies. The SIM setup was a prototype obtained from Carl Zeiss. Images were acquired with a 63× Plan-Apochromat (NA 1.4) with laser excitation at 488, 561, and 635 nm and then processed to obtain higher resolutions (Zen 2009; Carl Zeiss). For analysis of colocalization, Pearson's and Mander's coefficients were determined using the JACoP plugin of ImageJ v1.46r.

TIRF microscopy

The setup consisted of an inverted microscope (Optical IX70; Olympus), a solid-state laser system (85YCA010; Melles Griot) emitting at 561 nm, a TILL-TIRF condenser (T.I.L.L. Photonics), and an Acousto Optical Tunable Filter-nC (AA Opto-Electronic). The excitation/emission wavelengths were visualized with a dual-view camera splitter (Visitron Systems) to separate the red and green channels and a monochromator (Visichrome; Visitron Systems) to acquire images in epifluorescence. The setup was equipped with a camera (MicroMAX 512 BFT; Princeton Instruments) controlled by MetaMorph (Visitron Systems). A 100×/1.45 NA TIRF objective (Olympus Optical) was used. For some experiments, cells were imaged using a multiphoton confocal microscope (A1R; Nikon) with a 60×/1.49 NA Plan Apochromat objective using 488- and 561-nm lasers and a camera (iXon X3; Andor Technology). The exposure time was 100–150 ms. Experiments were performed at room temperature. Images were acquired using MetaMorph version 6.3 or NIS Elements (Nikon).

For live-cell imaging, human bead-stimulated CTLs were transfected with plasmids, washed, and resuspended in 30 µl AIM V medium and allowed to settle on anti-CD3– and anti-CD28–coated coverslips in an isotonic Ca^{2+}-free modified Ringer's solution (mM: 155 NaCl, 4.5 KCl, 5 Hepes, 2 $MgCl_2$, and 10 glucose; 300–310 osM). Cells were then perfused with modified Ringer's solution containing 10 mM Ca^{2+} to optimize Ca^{2+} influx during secretion and subsequently imaged for 15–20 min. Experiments were performed at room temperature.

Image analysis

Images and time-lapse series were analyzed using MetaMorph 6.3, ImageJ 1.46r, or the FIJI package of ImageJ. For vesicle dwell time and fusion analysis, analysis was performed with ImageJ 1.46r. Vesicles were defined as constituting 4–6 pixels. Dwell times in the TIRF plane were calculated manually for all vesicles in a cell. Cytotoxic granule fusion analysis was performed using ImageJ plugin Time Series Analyzer v.2.0. A sudden drop in the fluorescence within or <300 ms (three frames) was defined as a (fusion-like) fluorescence dispersion event.

Accumulation analysis was performed with ImageJ 1.46r. In brief, raw data files obtained from TIRF microscopy acquisitions were converted to 8 bits, and background was subtracted from the raw data of TIRF stacks using a Lipschitz filter with a top hat of 10. A threshold for vesicle accumulation was set as the mean gray value of background added 2 SD. The mean fluorescence of the area above threshold was obtained for every frame of the time-lapse video for each individual cell. A ratio was made between the threshold area and number of vesicles for a minimum of 10 frames for every cell (area/no. of vesicles = ratio). The threshold area was then divided by this ratio for all the time frames to get the number of vesicles for each frame. The mean number of vesicles in several cells was then plotted against the time (Pattu et al., 2011).

To quantify the F-actin clearance ratio at the immunological synapse, the MFI of the whole cell actin (MF1) was subtracted from the inner circular region of interest in the center of the immune synapse (MF2). Thus, a negative value indicates that the outer region has higher mean intensity than the inner region. The actin intensities were then divided by the actin footprint (MF1 × area of MF1) to normalize the data, averaged, and plotted against time.

Flow cytometric analyses of degranulation and Ca^{2+} flux

For evaluation of VAMP8 surface expression or cytotoxic granule exocytosis, human PBMCs were isolated from healthy donors by density gradient centrifugation (Lymphoprep). $CD8^+$ T cells were isolated from PBMCs by negative magnetic selection ($CD8^+$ negative isolation kit) and stimulated with antibody-coated beads (Dynabeads Human T-Activator CD3/CD28) in complete medium. The bead-stimulated CTLs were transfected with constructs encoding VAMP8-TFP, VAMP8-3×FLAG-TFP, or siRNA as indicated. CTLs were supplemented with 10 µg/ml anti-CD3 and 30 µg/ml anti-CD28 antibodies and mixed with P815 cells for the indicated time points at 37°C. Thereafter, the cells were surface stained on ice with fluorochrome-conjugated antibodies and analyzed by flow cytometry (LSR Fortessa; BD). FLAG expression was quantified on gated $CD3^+CD8^+TFP^+$ CTLs, and the frequency of $CD107a^+$ cells was determined among total $CD3^+CD8^+$ CTLs with FlowJo software (v.9.7.5; Tree Star).

For assessment of intracellular Ca^{2+} mobilization, bead-stimulated CTLs were incubated with 10 µg/ml anti-CD3 or IgG control antibody in 50 µl HBSS with Ca^{2+} and Mg^{2+} (Biosource) supplemented with 1% FBS for 30 min on ice. The cells were subsequently loaded with Fluo-4 and Fura red dyes on ice and prepared for flow cytometry as previously described (Bryceson et al., 2006). The cells were preincubated for 5 min at 37°C, and then, baseline was acquired on the flow cytometer for 30 s followed by addition of 5 µg goat anti–mouse $F(ab')_2$ antibodies (Jackson ImmunoResearch Laboratories, Inc.) and further flow cytometric evaluation. CTLs were gated on forward scatter/side scatter plots. The ratio between the MFI of FL-1 and FL-3 was calculated and plotted as a function of time using FlowJo software (v.9.7.5).

Assessment of ERK phosphorylation

After transfection with siRNA, human bead-stimulated CTL were incubated with 10 µg/ml anti-CD3 or isotype antibody in 50 µl HBSS with Ca^{2+} and Mg^{2+} (Biosource) supplemented with 1% FBS for 30 min on ice. The cells were washed, resuspended in RPMI 1640 supplemented with 10% FBS and 5 µg goat anti–mouse $F(ab')_2$ antibodies, incubated for 5 min at 37°C, spun, and lysed in boiling sample buffer (2× sample buffer, 4% β-mercaptoethanol, and 1 mM DTT) followed by sonication to disrupt and homogenize cells. The samples were subsequently incubated at 95°C for 5 min. Equivalent amounts of proteins were separated by SDS-PAGE and analyzed by Western blot.

Statistics

Statistical differences in data were analyzed with paired or unpaired *t* test, the Mann–Whitney U, or one-way analysis of variance (ANOVA) test, as specified, and graphed using Prism v.6 (GraphPad Software).

Online supplemental material

Fig. 1 shows colocalization of endogenous and ectopically expressed VAMP8. Fig. S2 shows that VAMP8 vesicles localize with Rab11a on recycling endosomal structures. Fig. S3 shows that VAMP8-carrying vesicles are rapidly recruited to and fuse with the plasma membrane at cytotoxic lymphocyte immune synapses. Fig. S4 shows that VAMP8 is not colocalized with granzyme B–containing granules. Fig. S5 shows that VAMP8 expression is strongly down-regulated and proximal TCR signaling is normal when VAMP8 expression in down-regulated by siRNA. Video 1 shows that VAMP8 accumulates and disperses at the immune synapse upon antigen receptor engagement. Video 2 shows that VAMP8 vesicles traffic and accumulate at the immune synapse with recycling endosomes markers upon antigen receptor engagement. Video 3 shows that VAMP8-carrying recycling endosomes are rapidly recruited to and fuse with the plasma membrane at immune synapses. Video 4 shows that VAMP8-carrying and perforin-containing vesicles have different spatial and temporal characteristics. Video 5 shows that VAMP8 and granzyme B have different spatial and temporal characteristics. Video 6 shows that recycling endosome fusion is inhibited upon knockdown of endogenous VAMP8 expression. Video 7 shows that cytotoxic granule fusion is inhibited upon knockdown of endogenous VAMP8 expression. Video 8 shows deposition of Stx11 and the immune synapse upon knockdown of endogenous VAMP8 expression. Online supplemental material is available at http://www.jcb.org/cgi/content/full/jcb.201411093/DC1.

ACKNOWLEDGEMENTS

We thank Dr. Ulf Matti, Dr. Bin Qu, and Dr. Mathias Laschke for help with statistical analysis and fruitful discussions. We thank Reiko Trautmann, Carolin Bick, Anne Weinland, Katrin Sandmeier, Anja Ludes, and Manuela Schneider for technical assistance. We thank Carmen Hässig and Claudia Kilter for expert cell preparation.

This project was funded by the Deutsche Forschungsgemeinschaft (RE1092/7-1 and SFB 894 to M. Hoth and J. Rettig), the European Research Council (ERC) under the European Union's Seventh Framework Programme (FP/2007-2013)/ERC grant agreement no. 311335, Swedish Research Council, Swedish Foundation for Strategic Research, Swedish Cancer Foundation, Swedish Children's Cancer Foundation, Knut and Alice Wallenberg Foundation, Histiocytosis Association, and the Karolinska Institute Research Foundation (to Y.T. Bryceson).

The authors declare no competing financial interests.

Author contributions: M.R. Marshall performed the majority of experiments shown in Figs.1–7 and S1–S5, V. Pattu contributed to the TIRF microscopy and analysis, M. Halimani performed the qRT-PCR experiments and assisted in the cloning of constructs, M. Maier-Peuschel performed various SIM and analysis, M.-L. Müller assisted in the cloning of constructs and Western blotting, W. Hong provided the VAMP8 antibody used in all confocal experiments, M. Hoth provided human cells and contributed to manuscript editing, T. Tschernig and U. Becherer contributed to technical advice on experimental design and manuscript editing, and M.R. Marshall, Y.T. Bryceson, and J. Rettig designed the experiments and wrote the manuscript.

Submitted: 20 November 2014
Accepted: 22 May 2015

References

Antonin, W., C. Holroyd, D. Fasshauer, S. Pabst, G.F. Von Mollard, and R. Jahn. 2000a. A SNARE complex mediating fusion of late endosomes defines conserved properties of SNARE structure and function. *EMBO J.* 19:6453–6464. http://dx.doi.org/10.1093/emboj/19.23.6453

Antonin, W., C. Holroyd, R. Tikkanen, S. Höning, and R. Jahn. 2000b. The R-SNARE endobrevin/VAMP-8 mediates homotypic fusion of early endosomes and late endosomes. *Mol. Biol. Cell.* 11:3289–3298. http://dx.doi.org/10.1091/mbc.11.10.3289

Barysch, S.V., S. Aggarwal, R. Jahn, and S.O. Rizzoli. 2009. Sorting in early endosomes reveals connections to docking- and fusion-associated factors. *Proc. Natl. Acad. Sci. USA.* 106:9697–9702. http://dx.doi.org/10.1073/pnas.0901444106

Bryceson, Y.T., M.E. March, H.G. Ljunggren, and E.O. Long. 2006. Synergy among receptors on resting NK cells for the activation of natural cytotoxicity and cytokine secretion. *Blood.* 107:159–166. http://dx.doi.org/10.1182/blood-2005-04-1351

Bryceson, Y.T., E. Rudd, C. Zheng, J. Edner, D. Ma, S.M. Wood, A.G. Bechensteen, J.J. Boelens, T. Celkan, R.A. Farah, et al. 2007. Defective cytotoxic lymphocyte degranulation in syntaxin-11 deficient familial hemophagocytic lymphohistiocytosis 4 (FHL4) patients. *Blood.* 110:1906–1915. http://dx.doi.org/10.1182/blood-2007-02-074468

Campi, G., R. Varma, and M.L. Dustin. 2005. Actin and agonist MHC–peptide complex–dependent T cell receptor microclusters as scaffolds for signaling. *J. Exp. Med.* 202:1031–1036. http://dx.doi.org/10.1084/jem.20051182

Chavrier, P., R.G. Parton, H.P. Hauri, K. Simons, and M. Zerial. 1990. Localization of low molecular weight GTP binding proteins to exocytic and endocytic compartments. *Cell.* 62:317–329. http://dx.doi.org/10.1016/0092-8674(90)90369-P

Chen, Y.A., and R.H. Scheller. 2001. SNARE-mediated membrane fusion. *Nat. Rev. Mol. Cell Biol.* 2:98–106. http://dx.doi.org/10.1038/35052017

Chiang, S.C., J. Theorell, M. Entesarian, M. Meeths, M. Mastafa, W. Al-Herz, P. Frisk, K.C. Gilmour, M. Ifversen, C. Langenskiöld, et al. 2013. Comparison of primary human cytotoxic T-cell and natural killer cell responses reveal similar molecular requirements for lytic granule exocytosis but differences in cytokine production. *Blood.* 121:1345–1356. http://dx.doi.org/10.1182/blood-2012-07-442558

Cichocki, F., H. Schlums, H. Li, V. Stache, T. Holmes, T.R. Lenvik, S.C. Chiang, J.S. Miller, M. Meeths, S.K. Anderson, and Y.T. Bryceson. 2014. Transcriptional regulation of Munc13-4 expression in cytotoxic lymphocytes is disrupted by an intronic mutation associated with a primary immunodeficiency. *J. Exp. Med.* 211:1079–1091. http://dx.doi.org/10.1084/jem.20131131

Côte, M., M.M. Ménager, A. Burgess, N. Mahlaoui, C. Picard, C. Schaffner, F. Al-Manjomi, M. Al-Harbi, A. Alangari, F. Le Deist, et al. 2009. Munc18-2 deficiency causes familial hemophagocytic lymphohistiocytosis type 5 and impairs cytotoxic granule exocytosis in patient NK cells. *J. Clin. Invest.* 119:3765–3773. http://dx.doi.org/10.1172/JCI40732

Das, V., B. Nal, A. Dujeancourt, M.I. Thoulouze, T. Galli, P. Roux, A. Dautry-Varsat, and A. Alcover. 2004. Activation-induced polarized recycling targets T cell antigen receptors to the immunological synapse; involvement of SNARE complexes. *Immunity.* 20:577–588. http://dx.doi.org/10.1016/S1074-7613(04)00106-2

de Saint Basile, G., G. Ménasché, and A. Fischer. 2010. Molecular mechanisms of biogenesis and exocytosis of cytotoxic granules. *Nat. Rev. Immunol.* 10:568–579. http://dx.doi.org/10.1038/nri2803

Douglass, A.D., and R.D. Vale. 2005. Single-molecule microscopy reveals plasma membrane microdomains created by protein-protein networks that exclude or trap signaling molecules in T cells. *Cell.* 121:937–950. http://dx.doi.org/10.1016/j.cell.2005.04.009

Dressel, R., L. Elsner, P. Novota, N. Kanwar, and G. Fischer von Mollard. 2010. The exocytosis of lytic granules is impaired in Vti1b- or Vamp8-deficient CTL leading to a reduced cytotoxic activity following antigen-specific activation. *J. Immunol.* 185:1005–1014. http://dx.doi.org/10.4049/jimmunol.1000770

Dustin, M.L., and E.O. Long. 2010. Cytotoxic immunological synapses. *Immunol. Rev.* 235:24–34. http://dx.doi.org/10.1111/j.0105-2896.2010.00904.x

Faroudi, M., C. Utzny, M. Salio, V. Cerundolo, M. Guiraud, S. Müller, and S. Valitutti. 2003. Lytic versus stimulatory synapse in cytotoxic T lymphocyte/target cell interaction: manifestation of a dual activation threshold. *Proc. Natl. Acad. Sci. USA.* 100:14145–14150. http://dx.doi.org/10.1073/pnas.2334336100

Feldmann, J., I. Callebaut, G. Raposo, S. Certain, D. Bacq, C. Dumont, N. Lambert, M. Ouachée-Chardin, G. Chedeville, H. Tamary, et al. 2003. Munc13-4 is essential for cytolytic granules fusion and is mutated in a form of familial hemophagocytic lymphohistiocytosis (FHL3). *Cell.* 115:461–473. http://dx.doi.org/10.1016/S0092-8674(03)00855-9

Gustafsson, M.G. 2005. Nonlinear structured-illumination microscopy: wide-field fluorescence imaging with theoretically unlimited resolution. *Proc. Natl. Acad. Sci. USA.* 102:13081–13086. http://dx.doi.org/10.1073/pnas.0406877102

Gustafsson, M.G., L. Shao, P.M. Carlton, C.J. Wang, I.N. Golubovskaya, W.Z. Cande, D.A. Agard, and J.W. Sedat. 2008. Three-dimensional resolution doubling in wide-field fluorescence microscopy by structured illumination. *Biophys. J.* 94:4957–4970. http://dx.doi.org/10.1529/biophysj.107.120345

Halimani, M., V. Pattu, M.R. Marshall, H.F. Chang, U. Matti, M. Jung, U. Becherer, E. Krause, M. Hoth, E.C. Schwarz, and J. Rettig. 2014. Syntaxin11 serves as a t-SNARE for the fusion of lytic granules in human cytotoxic T lymphocytes. *Eur. J. Immunol.* 44:573–584. http://dx.doi.org/10.1002/eji.201344011

Jahn, R., and R.H. Scheller. 2006. SNAREs—engines for membrane fusion. *Nat. Rev. Mol. Cell Biol.* 7:631–643. http://dx.doi.org/10.1038/nrm2002

Jenkins, M.R., A. Tsun, J.C. Stinchcombe, and G.M. Griffiths. 2009. The strength of T cell receptor signal controls the polarization of cytotoxic machinery to the immunological synapse. *Immunity.* 31:621–631. http://dx.doi.org/10.1016/j.immuni.2009.08.024

Kägi, D., B. Ledermann, K. Bürki, P. Seiler, B. Odermatt, K.J. Olsen, E.R. Podack, R.M. Zinkernagel, and H. Hengartner. 1994. Cytotoxicity mediated by T cells and natural killer cells is greatly impaired in perforin-deficient mice. *Nature.* 369:31–37. http://dx.doi.org/10.1038/369031a0

Kanwar, N., A. Fayyazi, B. Backofen, M. Nitsche, R. Dressel, and G.F. von Mollard. 2008. Thymic alterations in mice deficient for the SNARE protein VAMP8/endobrevin. *Cell Tissue Res.* 334:227–242. http://dx.doi.org/10.1007/s00441-008-0692-7

Krzewski, K., A. Gil-Krzewska, J. Watts, J.N. Stern, and J.L. Strominger. 2011. VAMP4- and VAMP7-expressing vesicles are both required for cytotoxic granule exocytosis in NK cells. *Eur. J. Immunol.* 41:3323–3329. http://dx.doi.org/10.1002/eji.201141582

Larghi, P., D.J. Williamson, J.M. Carpier, S. Dogniaux, K. Chemin, A. Bohineust, L. Danglot, K. Gaus, T. Galli, and C. Hivroz. 2013. VAMP7 controls T cell activation by regulating the recruitment and phosphorylation of vesicular Lat at TCR-activation sites. *Nat. Immunol.* 14:723–731. http://dx.doi.org/10.1038/ni.2609

Liu, D., Y.T. Bryceson, T. Meckel, G. Vasiliver-Shamis, M.L. Dustin, and E.O. Long. 2009. Integrin-dependent organization and bidirectional vesicular traffic at cytotoxic immune synapses. *Immunity.* 31:99–109. http://dx.doi.org/10.1016/j.immuni.2009.05.009

Loo, L.S., L.A. Hwang, Y.M. Ong, H.S. Tay, C.C. Wang, and W. Hong. 2009. A role for endobrevin/VAMP8 in CTL lytic granule exocytosis. *Eur. J. Immunol.* 39:3520–3528. http://dx.doi.org/10.1002/eji.200939378

Lopez, J.A., M.R. Jenkins, J.A. Rudd-Schmidt, A.J. Brennan, J.C. Danne, S.I. Mannering, J.A. Trapani, and I. Voskoboinik. 2013. Rapid and unidirectional perforin pore delivery at the cytotoxic immune synapse. *J. Immunol.* 191:2328–2334. http://dx.doi.org/10.4049/jimmunol.1301205

Matti, U., V. Pattu, M. Halimani, C. Schirra, E. Krause, Y. Liu, L. Weins, H.F. Chang, R. Guzman, J. Olausson, et al. 2013. Synaptobrevin2 is the v-SNARE required for cytotoxic T-lymphocyte lytic granule fusion. *Nat. Commun.* 4:1439. http://dx.doi.org/10.1038/ncomms2467

Maul-Pavicic, A., S.C.C. Chiang, A. Rensing-Ehl, B. Jessen, C. Fauriat, S.M. Wood, S. Sjöqvist, M. Hufnagel, I. Schulze, T. Bass, et al. 2011. ORAI1-mediated calcium influx is required for human cytotoxic lymphocyte degranulation and target cell lysis. *Proc. Natl. Acad. Sci. USA.* 108:3324–3329. http://dx.doi.org/10.1073/pnas.1013285108

Ménager, M.M., G. Ménasché, M. Romao, P. Knapnougel, C.H. Ho, M. Garfa, G. Raposo, J. Feldmann, A. Fischer, and G. de Saint Basile. 2007. Secretory cytotoxic granule maturation and exocytosis require the effector protein hMunc13-4. *Nat. Immunol.* 8:257–267. http://dx.doi.org/10.1038/ni1431

Miesenböck, G., D.A. De Angelis, and J.E. Rothman. 1998. Visualizing secretion and synaptic transmission with pH-sensitive green fluorescent proteins. *Nature.* 394:192–195. http://dx.doi.org/10.1038/28190

Pattu, V., B. Qu, M. Marshall, U. Becherer, C. Junker, U. Matti, E.C. Schwarz, E. Krause, M. Hoth, and J. Rettig. 2011. Syntaxin7 is required for lytic granule release from cytotoxic T lymphocytes. *Traffic.* 12:890–901. http://dx.doi.org/10.1111/j.1600-0854.2011.01193.x

Pattu, V., B. Qu, E.C. Schwarz, B. Strauss, L. Weins, S.S. Bhat, M. Halimani, M. Marshall, J. Rettig, and M. Hoth. 2012. SNARE protein expression and localization in human cytotoxic T lymphocytes. *Eur. J. Immunol.* 42:470–475. http://dx.doi.org/10.1002/eji.201141915

Paumet, F., J. Le Mao, S. Martin, T. Galli, B. David, U. Blank, and M. Roa. 2000. Soluble NSF attachment protein receptors (SNAREs) in RBL-2H3 mast cells: functional role of syntaxin 4 in exocytosis and identification of a vesicle-associated membrane protein 8-containing secretory compartment. *J. Immunol.* 164:5850–5857. http://dx.doi.org/10.4049/jimmunol.164.11.5850

Purbhoo, M.A., D.J. Irvine, J.B. Huppa, and M.M. Davis. 2004. T cell killing does not require the formation of a stable mature immunological synapse. *Nat. Immunol.* 5:524–530. http://dx.doi.org/10.1038/ni1058

Puri, N., and P.A. Roche. 2008. Mast cells possess distinct secretory granule subsets whose exocytosis is regulated by different SNARE isoforms. *Proc. Natl. Acad. Sci. USA.* 105:2580–2585. http://dx.doi.org/10.1073/pnas.0707854105

Qu, B., V. Pattu, C. Junker, E.C. Schwarz, S.S. Bhat, C. Kummerow, M. Marshall, U. Matti, F. Neumann, M. Pfreundschuh, et al. 2011. Docking of lytic granules at the immunological synapse in human CTL requires Vti1b-dependent pairing with CD3 endosomes. *J. Immunol.* 186:6894–6904. http://dx.doi.org/10.4049/jimmunol.1003471

Rak, G.D., E.M. Mace, P.P. Banerjee, T. Svitkina, and J.S. Orange. 2011. Natural killer cell lytic granule secretion occurs through a pervasive actin network at the immune synapse. *PLoS Biol.* 9:e1001151. http://dx.doi.org/10.1371/journal.pbio.1001151

Ren, Q., H.K. Barber, G.L. Crawford, Z.A. Karim, C. Zhao, W. Choi, C.C. Wang, W. Hong, and S.W. Whiteheart. 2007. Endobrevin/VAMP-8 is the primary v-SNARE for the platelet release reaction. *Mol. Biol. Cell.* 18:24–33. http://dx.doi.org/10.1091/mbc.E06-09-0785

Riedl, J., A.H. Crevenna, K. Kessenbrock, J.H. Yu, D. Neukirchen, M. Bista, F. Bradke, D. Jenne, T.A. Holak, Z. Werb, et al. 2008. Lifeact: a versatile marker to visualize F-actin. *Nat. Methods.* 5:605–607. http://dx.doi.org/10.1038/nmeth.1220

Rybin, V., O. Ullrich, M. Rubino, K. Alexandrov, I. Simon, M.C. Seabra, R. Goody, and M. Zerial. 1996. GTPase activity of Rab5 acts as a timer for endocytic membrane fusion. *Nature.* 383:266–269. http://dx.doi.org/10.1038/383266a0

Sander, L.E., S.P. Frank, S. Bolat, U. Blank, T. Galli, H. Bigalke, S.C. Bischoff, and A. Lorentz. 2008. Vesicle associated membrane protein (VAMP)-7 and VAMP-8, but not VAMP-2 or VAMP-3, are required for activation-induced degranulation of mature human mast cells. *Eur. J. Immunol.* 38:855–863. http://dx.doi.org/10.1002/eji.200737634

Soares, H., R. Henriques, M. Sachse, L. Ventimiglia, M.A. Alonso, C. Zimmer, M.I. Thoulouze, and A. Alcover. 2013. Regulated vesicle fusion generates signaling nanoterritories that control T cell activation at the immunological synapse. *J. Exp. Med.* 210:2415–2433. http://dx.doi.org/10.1084/jem.20130150

Stepp, S.E., R. Dufourcq-Lagelouse, F. Le Deist, S. Bhawan, S. Certain, P.A. Mathew, J.I. Henter, M. Bennett, A. Fischer, G. de Saint Basile, and V. Kumar. 1999. Perforin gene defects in familial hemophagocytic lymphohistiocytosis. *Science.* 286:1957–1959. http://dx.doi.org/10.1126/science.286.5446.1957

Stinchcombe, J.C., and G.M. Griffiths. 2007. Secretory mechanisms in cell-mediated cytotoxicity. *Annu. Rev. Cell Dev. Biol.* 23:495–517. http://dx.doi.org/10.1146/annurev.cellbio.23.090506.123521

Stinchcombe, J.C., E. Majorovits, G. Bossi, S. Fuller, and G.M. Griffiths. 2006. Centrosome polarization delivers secretory granules to the immunological synapse. *Nature.* 443:462–465. http://dx.doi.org/10.1038/nature05071

Stow, J.L. 2013. Nobel Prize discovery paves the way for immunological traffic. *Nat. Rev. Immunol.* 13:839–841. http://dx.doi.org/10.1038/nri3564

Stow, J.L., A.P. Manderson, and R.Z. Murray. 2006. SNAREing immunity: the role of SNAREs in the immune system. *Nat. Rev. Immunol.* 6:919–929. http://dx.doi.org/10.1038/nri1980

Südhof, T.C., and J.E. Rothman. 2009. Membrane fusion: grappling with SNARE and SM proteins. *Science.* 323:474–477. http://dx.doi.org/10.1126/science.1161748

Sutton, R.B., D. Fasshauer, R. Jahn, and A.T. Brunger. 1998. Crystal structure of a SNARE complex involved in synaptic exocytosis at 2.4 A resolution. *Nature.* 395:347–353. http://dx.doi.org/10.1038/26412

Sykulev, Y., M. Joo, I. Vturina, T.J. Tsomides, and H.N. Eisen. 1996. Evidence that a single peptide-MHC complex on a target cell can elicit a cytolytic T cell response. *Immunity.* 4:565–571. http://dx.doi.org/10.1016/S1074-7613(00)80483-5

Trapani, J.A., and M.J. Smyth. 2002. Functional significance of the perforin/granzyme cell death pathway. *Nat. Rev. Immunol.* 2:735–747. http://dx.doi.org/10.1038/nri911

Ullrich, O., S. Reinsch, S. Urbé, M. Zerial, and R.G. Parton. 1996. Rab11 regulates recycling through the pericentriolar recycling endosome. *J. Cell Biol.* 135:913–924. http://dx.doi.org/10.1083/jcb.135.4.913

Ungermann, C., and D. Langosch. 2005. Functions of SNAREs in intracellular membrane fusion and lipid bilayer mixing. *J. Cell Sci.* 118:3819–3828. http://dx.doi.org/10.1242/jcs.02561

Wang, C.C., C.P. Ng, L. Lu, V. Atlashkin, W. Zhang, L.F. Seet, and W. Hong. 2004. A role of VAMP8/endobrevin in regulated exocytosis of pancreatic acinar cells. *Dev. Cell.* 7:359–371. http://dx.doi.org/10.1016/j.devcel.2004.08.002

Wong, S.H., T. Zhang, Y. Xu, V.N. Subramaniam, G. Griffiths, and W. Hong. 1998. Endobrevin, a novel synaptobrevin/VAMP-like protein preferentially associated with the early endosome. *Mol. Biol. Cell.* 9:1549–1563. http://dx.doi.org/10.1091/mbc.9.6.1549

Yokosuka, T., K. Sakata-Sogawa, W. Kobayashi, M. Hiroshima, A. Hashimoto-Tane, M. Tokunaga, M.L. Dustin, and T. Saito. 2005. Newly generated T cell receptor microclusters initiate and sustain T cell activation by recruitment of Zap70 and SLP-76. *Nat. Immunol.* 6:1253–1262. http://dx.doi.org/10.1038/ni1272

zur Stadt, U., S. Schmidt, B. Kasper, K. Beutel, A.S. Diler, J.I. Henter, H. Kabisch, R. Schneppenheim, P. Nürnberg, G. Janka, and H.C. Hennies. 2005. Linkage of familial hemophagocytic lymphohistiocytosis (FHL) type-4 to chromosome 6q24 and identification of mutations in syntaxin 11. *Hum. Mol. Genet.* 14:827–834. http://dx.doi.org/10.1093/hmg/ddi076

zur Stadt, U., J. Rohr, W. Seifert, F. Koch, S. Grieve, J. Pagel, J. Strauss, B. Kasper, G. Nürnberg, C. Becker, et al. 2009. Familial hemophagocytic lymphohistiocytosis type 5 (FHL-5) is caused by mutations in Munc18-2 and impaired binding to syntaxin 11. *Am. J. Hum. Genet.* 85:482–492. http://dx.doi.org/10.1016/j.ajhg.2009.09.005